5. Conclusions

Infectious HCV could be efficiently produced in serum-free culture. However, the serum-free cultured HCV was highly susceptible to anti-CD81, anti-SR-BI and anti-E2 inhibition of infectivity. The content of ApoB and ApoE in HCV from serum-supplemented and serum-free cultures was different and the infectivity of serum-free cultured HCV appeared to be independent of apolipoproteins. Therefore, lipids conjugated with HCV may affect virus infection and neutralization.

Acknowledgements

This work was partially supported by a grant-in-aid for Scientific Research from the Japan Society for the Promotion of Science and from the Ministry of Health, Labor, and Welfare of Japan by the Research on Health Sciences Focusing on Drug Innovation from the Japan Health Sciences Foundation. Huh7.5.1 was a kind gift from Dr. Francis V. Chisari. Anti-SR-BI antibody and rat serum were kind gifts from Dr. H. Barth. Antibody AP33 was a kind gift from Genentech, Inc.

Appendix A. Supplementary data

Supplementary data associated with this article can be found, in the online version, at doi:10.1016/j.vaccine.2011.04.069.

References

[1] Kato T, Date T, Miyamoto M, Furusaka A, Tokushige K, Mizokami M, et al. Efficient replication of the genotype 2a hepatitis C virus subgenomic replicon. Gastroenterology 2003;125:1808–17.
[2] Wakita T, Pietschmann T, Kato T, Date T, Miyamoto M, Zhao Z, et al. Production of infectious hepatitis C virus in tissue culture from a cloned viral genome. Nat Med 2005;11:791–6.
[3] Lindenbach BD, Evans MJ, Syder AJ, Wolk B, Tellinghuisen TL, Liu CC, et al. Complete replication of hepatitis C virus in cell culture. Science 2005;309:623–6.
[4] Zhong J, Gastaminza P, Cheng G, Kapadia S, Kato T, Burton DR, et al. Robust hepatitis C virus infection in vitro. Proc Natl Acad Sci USA 2005;102:9294–9.
[5] Gottwein JM, Scheel TK, Jensen TB, Lademann JB, Prentoe JC, Knudsen ML, et al. Development and characterization of hepatitis C virus genotype 1–7 cell culture systems: role of CD81 and scavenger receptor class B type I and effect of antiviral drugs. Hepatology 2009;49:364–77.
[6] Nakabayashi H, Taketa K, Miyano K, Yamane T, Sato J. Growth of human hepatoma cells lines with differentiated functions in chemically defined medium. Cancer Res 1982;42:3858–63.
[7] Andre P, Komurian-Pradel F, Deforges S, Perret M, Berland JL, Sodoyer M, et al. Characterization of low- and very-low-density hepatitis C virus RNA-containing particles. J Virol 2002;76:6919–28.
[8] Nielsen SU, Bassendine MF, Burt AD, Martin C, Pumeechockchai W, Toms GL. Association between hepatitis C virus and very-low-density lipoprotein (VLDL)/LDL analyzed in iodixanol density gradients. J Virol 2006;80:2418–28.
[9] Nielsen SU, Bassendine MF, Martin C, Lowther D, Purcell PJ, King BJ, et al. Characterization of hepatitis C RNA-containing particles from human liver by density and size. J Gen Virol 2008;89:2507–17.
[10] Gastaminza P, Dryden K, Boyd B, Wood M, Law M, Yeager M, et al. Ultrastructural and biophysical characterization of hepatitis C virus particles produced in cell culture. J Virol 2010;84:10999–1009.
[11] Masciopinto F, Giovani C, Campagnoli S, Galli-Stampino L, Colombatto P, Brunetto M, et al. Association of hepatitis C virus envelope proteins with exosomes. Eur J Immunol 2004;34:2834–42.
[12] Akazawa D, Date T, Morikawa K, Murayama A, Miyamoto M, Kaga M, et al. CD81 expression is important for the permissiveness of Huh7 cell clones for heterogeneous hepatitis C virus infection. J Virol 2007;81:5036–45.
[13] Murayama A, Date T, Morikawa K, Akazawa D, Miyamoto M, Kaga M, et al. The NS3 helicase and NS5B-to-3′X regions are important for efficient hepatitis C virus strain JFH-1 replication in Huh7 cells. J Virol 2007;81:8030–40.
[14] Kato T, Date T, Murayama A, Morikawa K, Akazawa D, Wakita T. Cell culture and infection system for hepatitis C virus. Nat Protoc 2006;1:2334–9.
[15] Date T, Miyamoto M, Kato T, Morikawa K, Murayama A, Akazawa D, et al. An infectious and selectable full-length replicon system with hepatitis C virus JFH-1 strain. Hepatol Res 2007;37:433–43.
[16] Barth H, Cerino R, Arcuri M, Hoffmann M, Schürmann P, Adah MI, et al. Scavenger receptor class B type I and hepatitis C virus infection of primary Tupaia hepatocytes. J Virol 2005;79:5774–85.
[17] Murakami K, Kimura T, Osaki M, Ishii K, Miyamura T, Suzuki T, et al. Virological characterization of the hepatitis C virus JFH-1 strain in lymphocytic cell lines. J Gen Virol 2008;89:1587–92.
[18] Takeuchi T, Katsume A, Tanaka T, Abe A, Inoue K, Tsukiyama-Kohara K, et al. Real-time detection system for quantification of hepatitis C virus genome. Gastroenterology 1999;116:636–42.
[19] Kato T, Choi Y, Elmowalid G, Sapp RK, Barth H, Furusaka A, et al. Hepatitis C virus JFH-1 strain infection in chimpanzees is associated with low pathogenicity and emergence of an adaptive mutation. Hepatology 2008;48:732–40.
[20] Owsianka A, Tarr AW, Juttla VS, Lavillette D, Bartosch B, Cosset FL, et al. Monoclonal antibody AP33 defines a broadly neutralizing epitope on the hepatitis C virus E2 envelope glycoprotein. J Virol 2005;79:11095–104.
[21] Tarr AW, Owsianka AM, Timms JM, McClure CP, Brown RJ, Hickling TP, et al. Characterization of the hepatitis C virus E2 epitope defined by the broadly neutralizing monoclonal antibody AP33. Hepatology 2006;43:592–601.
[22] Gastaminza P, Cheng G, Wieland S, Zhong J, Liao W, Chisari FV. Cellular determinants of hepatitis C virus assembly, maturation, degradation, and secretion. J Virol 2008;82:2120–9.
[23] Huang H, Sun F, Owen DM, Li W, Chen Y, Gale Jr M, et al. Hepatitis C virus production by human hepatocytes dependent on assembly and secretion of very low-density lipoproteins. Proc Natl Acad Sci USA 2007;104:5848–53.
[24] Zhong J, Gastaminza P, Chung J, Stamataki Z, Isogawa M, Cheng G, et al. Persistent hepatitis C virus infection in vitro: coevolution of virus and host. J Virol 2006;80:11082–93.
[25] Thomssen R, Bonk S, Propfe C, Heermann KH, Kochel HG, Uy A. Association of hepatitis C virus in human sera with beta-lipoprotein. Med Microbiol Immunol 1992;181:293–300.
[26] Monazahian M, Kippenberger S, Muller A, Seitz H, Bohme I, Grethe S, et al. Binding of human lipoproteins (low, very low, high density lipoproteins) to recombinant envelope proteins of hepatitis C virus. Med Microbiol Immunol 2000;188:177–84.
[27] Benga WJ, Krieger SE, Dimitrova M, Zeisel MB, Parnot M, Lupberger J, et al. Apolipoprotein E interacts with hepatitis C virus nonstructural protein 5A and determines assembly of infectious particles. Hepatology 2010;51:43–53.
[28] Chang KS, Jiang J, Cai Z, Luo G. Human apolipoprotein E is required for infectivity and production of hepatitis C virus in cell culture. J Virol 2007;81:13783–93.
[29] Jiang J, Luo G. Apolipoprotein E but not B is required for the formation of infectious hepatitis C virus particles. J Virol 2009;83:12680–91.

Virus Research 157 (2011) 116–120

Contents lists available at ScienceDirect

Virus Research

journal homepage: www.elsevier.com/locate/virusres

Short communication

An SV40 mutant defective in VP4 expression exhibits a temperature-sensitive growth defect

Shoichiro Tange, Takeshi Imai, Akira Nakanishi *

National Center for Geriatrics and Gerontology, Obu, Aichi 474-8522, Japan

ARTICLE INFO

Article history:
Received 14 October 2010
Received in revised form 1 February 2011
Accepted 1 February 2011
Available online 16 February 2011

Keywords:
Polyomavirus
SV40
Vp4
Temperature sensitive phenotype

ABSTRACT

On reexamination of temperature-sensitive D-type (tsD) mutants of simian virus 40 (SV40), we found that the tsD222 mutant is identical to the VP2 M228I mutant, which is defective in VP4 expression, at the nucleotide level. Although a previous study reported that lack of VP4 caused defects in viral dissemination in BSC-1 cells, this mutant showed a temperature-sensitive growth defect in CV-1 cells. tsD101:VP3 Q113K and tsD202:VP3 P108S exhibited a growth phenotype similar to that of tsD222, and they retained the VP4 open reading frame (ORF). These three mutants did not complement each other, suggesting that their defects were functionally indistinguishable. Transduction of the SV40 vector expressing wild-type VP4 in tsD222-infected cells did not ameliorate the growth defect at the non-permissive temperature. The results indicate that tsD mutation in minor capsid proteins has a more profound impact on viral propagation, and that lack of VP4 ORF seems to have little influence on viral growth.

Simian virus 40 (SV40), which belongs to the family *Polyomaviridae*, is a small DNA tumor virus with a circular, double-stranded DNA genome. Its capsid is composed of 360 VP1 major capsid proteins and approximately 72 VP2 and VP3 (VP2/3) minor capsid proteins. These two minor capsid proteins are encoded by the same mRNA and reading frame, but they differ in their translational start site; thus, VP2 is 118 residues longer than VP3. The open reading frame (ORF) for the minor capsid proteins harbors a small non-structural protein, VP4, of approximately 15 kDa. The translational initiation site of VP4 is downstream of the VP3 initiation codon and it functions during viral lysis by facilitating the release of progeny virions (Daniels et al., 2007).

Minor capsid proteins are involved in the post-entry event during viral infection, i.e., during the intracellular trafficking and nuclear import of the viral genome (Nakanishi et al., 2006; Nakanishi et al., 2002). The original concept came from early studies of SV40 using temperature-sensitive D-type (tsD) SV40 mutants (Avila et al., 1976; Chou et al., 1974; Chou and Martin, 1974; Robb and Martin, 1972) in which mutations were physically mapped to the VP3 coding region between SV40 nucleotide number (SV40 nt) (Reddy et al., 1978) 1046 and 1493 (Lai and Nathans, 1975a; Lai and Nathans, 1975b; Shenk et al., 1975). These mutants were apparently defective in the uncoating process in which the initiation of viral gene expression on infection was blocked at the restrictive, non-permissive temperature, although their viral DNA was completely capable of initiating viral growth on transfection. We aimed to reexamine tsD mutants to determine whether such a phenotype could help us identify the domain that is important for viral uncoating, but instead we found that one of the tsD mutants is identical to that defective in VP4 expression.

Nucleotide alterations in tsD101, tsD202, and tsD222 (Chou and Martin, 1974; Robb and Martin, 1972) were identified as SV40 nt 1252C to A, 1237C to T, and 1245G to A, respectively (Fig. 1A) by sequencing the region encompassing VP3 coding region, from SV40 nt 900 to 1792, amplified with Herculase polymerase (Stratagene, La Jolla, CA), which has proofreading activity, using the respective mutant viral lysate as the template and the primers, 5′-ATATCAACAACCAGGAATGGCT-3′ and 5′-CAAAGGAATTCTAGCCACACTGTAGCA-3′. The amino acid changes were VP3 108 Pro to Ser (P108S) in tsD202, VP3 113 Gln to Lys (Q113K) in tsD101, and VP3 110 Met to Ile (M110I) in tsD222 (Fig. 1A). The mutations appeared to be clustered together on the amino-terminal side of the VP1-interactive domain of VP3 (Chen et al., 1998; Nakanishi et al., 2006), implying the presence of a functional domain. We note that nucleotide change in tsD222, VP3 M110I, is identical to that of VP2 M228I. This particular mutant is shown to be defective in VP4 expression and blocked in viral dissemination in BSC-1 cells (Daniels et al., 2007).

To confirm whether these mutations result in a temperature-sensitive phenotype, each individual nucleotide alteration as well as the combination of the three mutations, VP3 P108S-M110I-Q113K (PMQ/SIK), were introduced into an infectious molecular

* Corresponding author at: Section of Gene Therapy, Department of Aging Intervention, National Center for Geriatrics and Gerontology, 35 Gengo, Morioka, Obu, Aichi 474-8522, Japan. Tel.: +81 562 44 5651x5058; fax: +81 562 46 8461.
E-mail address: nakanish@ncgg.go.jp (A. Nakanishi).

0168-1702/$ – see front matter © 2011 Elsevier B.V. All rights reserved.
doi:10.1016/j.virusres.2011.02.001

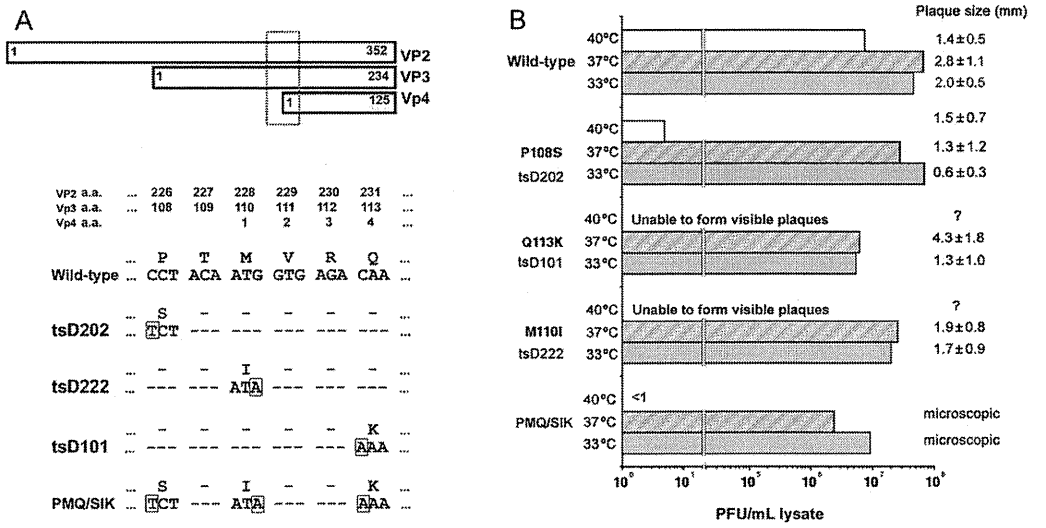

Fig. 1. Nucleotide alterations in SV40 tsD mutants resulting in temperature-sensitive phenotypes. (A) Nucleotide alterations in SV40 tsD mutants: The upper panel shows a schematic diagram of the VP2, VP3, and VP4 coding regions. The lower panel shows the nucleotide sequence of SV40 nt 1237 to 1254 encoding the partial open reading frame of the VP2, VP3, and VP4. The corresponding VP2, VP3, and VP4 amino acid numbers are indicated. Nucleotide alterations in tsD202, tsD222, tsD101, and PMQ/SIK are boxed and the resultant amino acid changes are shown. (B) Plaque assay of mutants introduced with the nucleotide alteration found in tsD mutants: Lysates of CV-1 cells transfected with the respective viral DNA were quantified for viral DNA using real-time quantitative PCR targeted to the SV40 origin sequence using SYBR Green Realtime PCR Master Mix Plus (Toyobo) and the primers, 5′-AAGCCTCCTCACTACTTCTGGAATAGCTC-3′ and 5′-AGCATGCATCTCAATTAGTCAGCAACCATA-3′, operated using LightCycler (Roche Applied Biosciences, Basel, Switzerland), and adjusted to contain 2.0×10^{11} viral DNA/mL as described (Nakanishi et al., 2008). The lysates were serially diluted, applied to CV-1 cells incubated at 40 °C (open column), 37 °C (shaded column), or 33 °C (dotted column), and stained for plaques (Nakanishi et al., 2002). Plaque-forming units (PFUs) present in the 1-mL cell lysate containing approximately 2.0×10^{11} viral DNA are shown as columns. Numbers shown at the side of the columns indicate mean plaque size ± standard deviation (mm).

clone of SV40, NOpSV40 SRBSM (Li et al., 2003), and pSV40, which harbors the natural SV40 genome, using *Sal*I and *Rsr*II and *Eco*RV and *Afl*II, respectively. Both types of viral DNA were excised by digestion with *Bam*HI and religated to generate infectious viral DNA (Ishii et al., 1994). Unless otherwise noted the results presented below are from experiments using viral DNA derived from NOpSV40. Upon DNA transfection into the CV-1 and BSC-1 cell lines, the extent of viral DNA replication and capsid protein expression at 72-h after transfection was similar among the mutants, including PMQ/SIK and the wild-type virus, irrespective of the cell type or temperature (40 °C or 37 °C) (Supplemental Fig. S1), which is consistent with previous results showing that DNA of tsD mutants were fully infectious (Chou and Martin, 1975; Daniels et al., 2007; Robb and Martin, 1972). Viral lysates, prepared by transfecting the respective viral DNA into CV-1 cells, were used to test viability of the viruses by infecting CV-1 cells in the plaque assay (Fig. 1B). At permissive temperatures (33 °C or 37 °C), all mutants except for PMQ/SIK produced similar number of plaques as that produced by the wild-type virus (Fig. 1B). PMQ/SIK produced very small plaques that were only discernable under a microscope. At restrictive temperatures (40 °C), all mutants were defective in plaque production, thereby confirming the temperature-sensitive phenotype of these mutants. At a high multiplicity of infection (MOI), infection with Q113K or M110I resulted in a cytopathic effect in most cells, although no visible plaques were present at lower MOIs (Supplemental Fig. S2). P108S produced 10^7-fold less plaques at 40 °C, and PMQ/SIK was nonviable at 40 °C.

When natural SV40 was used as the parental genome, the viability of the mutant harboring M110I or Q113K mutations at 40 °C was approximately 10^2-fold less than that at 33 °C (Supplemental Table S1), whereas approximately 10^3- to 10^4-fold less viability was observed in the previous study (Chou and Martin, 1974). We also noticed that NOSV40 grew more slowly than natural SV40, though the difference was not much pronounced (data not shown). Such minor growth delays might emphasize the mutant's phenotype, i.e., defective in growth at the non-permissive temperature or in BSC-1 cells (discussed below). Although the extent of decrease in viability varies among parental plasmids or experiments, M110I, Q113K, and P108S mutations apparently resulted in the temperature-sensitive phenotype in CV-1 cells (Fig. 1B).

Since the mutants were originally identified by their inability to initiate viral DNA replication on infection at non-permissive temperatures (Chou and Martin, 1975), they were examined at the onset of viral gene expression in CV-1 cells at 37 °C or 40 °C, as well as in BSC-1 cells at 37 °C. The experiments hereafter were performed at 37 °C, considering 37 °C as the permissive temperature because we consistently observed that viability at 33 °C and 37 °C was identical. Cell lysates containing viral particles were adjusted to contain 2.0×10^{11} copies of viral DNA/mL (see Fig. 1B legend) and were used for infecting the cells applying about thousand viral DNA to each cell. When examined for T antigen expression at 60-h after infection (hours post-infection, hpi) by Western blot, the T antigen signal was detected only in wild-type-infected CV-1 cells incubated at both temperatures (Fig. 2A, upper panel). A very faint signal was detected in Q113K-infected CV-1 cells incubated at 37 °C, while the signal in wild-type-infected BSC-1 cells and the remaining mutant-infected cells was undetectable. To employ a more sensitive approach, T antigen expression was detected by immunofluorescence staining of the infected cells (Fig. 2B). On infection with wild-type viruses, almost all cells became T antigen positive at 60 hpi, while mutant-infected cells exhibited a lower proportion of T antigen-positive cells, irrespective of cell type or temperature (Fig. 2B). M110I-infected cells exhibited approximately 50% positive cells, while Q113K-infected cells were 50–75% positive for T antigen expression. P108- and PMQ/SIK-infected cells showed a much lower proportion of T antigen-positive cells; approximately 25% for P108-infected cells and <10% for PMQ/SIK-infected cells. Notably, the signal in BSC-1 cells tended to be weak compared with that in CV-1 cells, which may explain why the Western blot signal from BSC-1 cells was much lower than that from CV-1 cells. Thus, all mutants exhibited defects in viral gene expression under all conditions examined, and these data were consistent

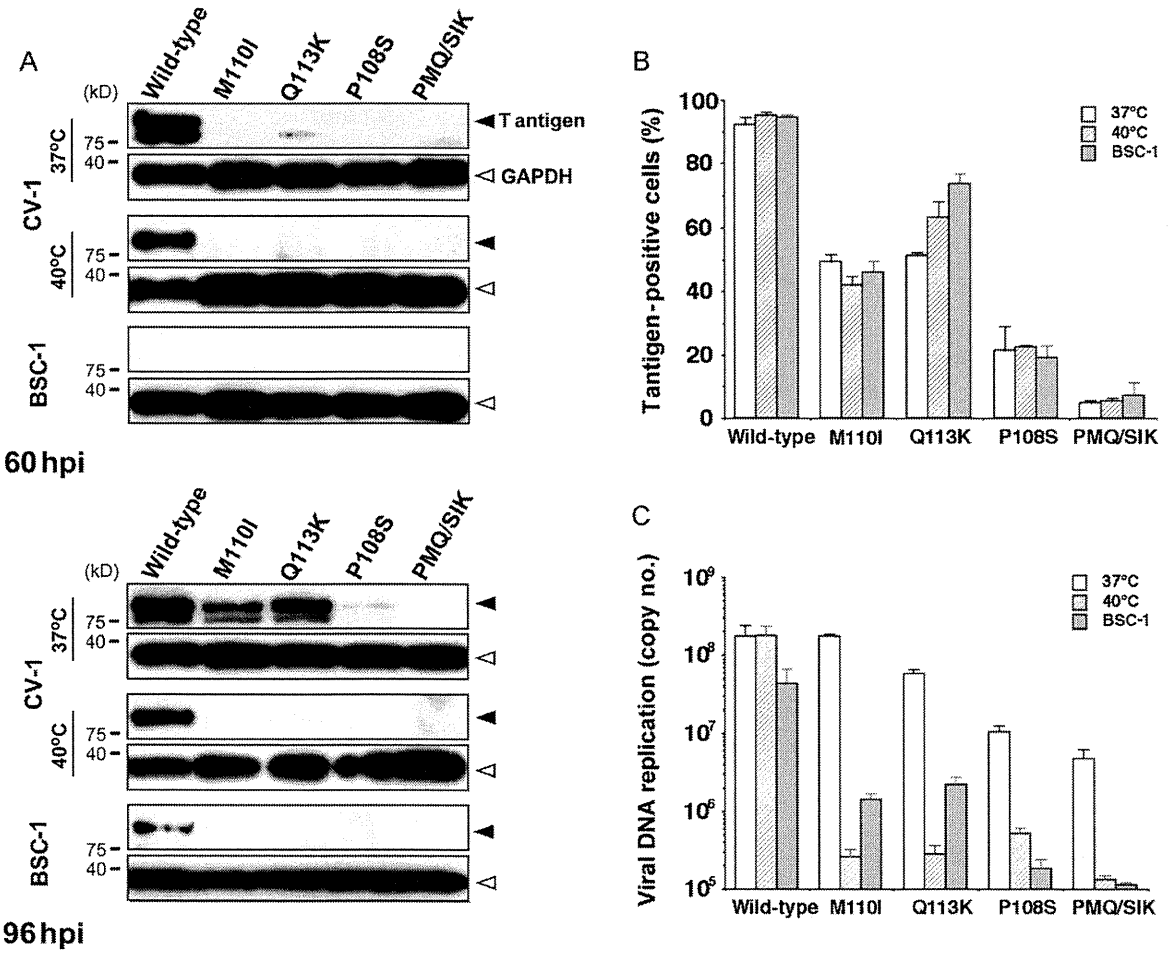

Fig. 2. Viral gene expression and viral DNA replication of mutants harboring tsD mutations. (A) Western blot detection of T antigen expression on infection with mutants: CV-1 or BSC-1 cells infected with either wild-type or the mutant were harvested for detecting the T antigen by Western blot at 60 h hpi (upper panel) or 96 hpi (lower panel). Approximately half of the cells harvested from individual six-well plates were used for detecting the SV40 T antigen using mouse monoclonal anti-T antigen (PAb419; Oncogene Sci., USA) as the primary antibody and peroxidase-conjugated anti-mouse IgG antibody (GE Healthcare, Bucks, UK) as the secondary antibody followed by enzyme chemiluminescence (ECL) (Immunostar; Wako chemicals, Osaka, Japan). As a loading control, glyceraldehyde-3-phosphate dehydrogenase (GAPDH) was detected using mouse anti-GAPDH antibody (clone 6C5; Millipore, Billerica, MA, USA) by ECL similar to the T antigen. Note that wild-type-infected cells tended to have lower amounts of protein because of an effective blockage of cell growth on infection, whereas the mutant-infected cells were less interfered with the growth likely due to lower incident of viral infection or lower level of viral gene expression. Positions of molecular weight markers for 75 and 45 kDa as well as those of the T antigen (filled arrowhead) and GAPDH (open arrowhead) are indicated. (B) Immunofluorescence detection of T antigen expression on infection: Cell lysates containing viral particles, adjusted for viral DNA as in the plaque assay (Fig. 1B), were used to infect CV-1 cells incubated at 37 °C (open columns) or 40 °C (shaded columns), and to BSC-1 cells incubated at 37 °C (closed columns). At 60 hpi, the cells were fixed, and the proportion of T antigen-positive cells were examined by immunocytochemistry using mouse monoclonal anti-T antigen antibody and Alexa Fluor 488-conjugated goat anti-mouse IgG antibody (Molecular probes, Eugene, OR, USA). (C) Viral DNA replication on infection with mutants: The cells infected as described in Fig. 2B were extracted for low molecular weight DNA at 96 hpi as described (Nakanishi et al., 2006). The extracted DNA was quantified for SV40 DNA as described in Fig. 1B. The columns are designated as shown in Fig. 2B. The amount of viral DNA shown is the mean value of the triplicate with standard deviation as indicated.

with those obtained by Western blot detection of T antigen expression (Fig. 2A, upper panel).

When T antigen expression was examined for the lysate obtained at 96 hpi by Western blot, the comparable signal was detected in wild-type-, M110I-, and Q113K-infected CV-1 cells grown at permissive temperature. The lysate from wild-type-infected CV-1 cells grown at 40 °C and BSC-1 cells at 37 °C also contained detectable T antigen, while the signal was mostly undetected in mutant-infected CV-1 cells grown at 40 °C and in BSC-1 cells. Similarly, the extent of viral DNA replication examined by quantitative PCR showed that the levels of viral DNA in M110I- and Q113K-infected CV-1 cells grown at 37 °C were comparable with those in wild-type-infected cells, while a much lower extent of DNA replication was observed when the cells were incubated at 40 °C or in BSC-1 cells infected with the respective mutants (Fig. 2C). The growth of the mutants P108S and PMQ/SIK was affected by the mutation in CV-1 cells even grown at 37 °C and severely blocked at 40 °C and in BSC-1 cells. We note that viral growth in mutant-infected BSC-1 cells was similar to that in mutant-infected CV-1 cells at non-permissive temperature. Viral DNA replication in BSC-1 cells is known to be initiated 10–20 h later than that in CV-1 cells (Ritzi and Levine, 1970). Such slower viral growth in BSC-1 cells could make the mutants' growth defect more apparent similar to that in CV-1 cells grown at 40 °C. These results indicated that, similar to the previous observations using the mutants with natural SV40 backbone, the mutants showed growth defect in CV-1 cells at non-permissive temperature and in BSC-1 cells. P108S mutation appeared to affect viral gene expression and DNA replication more severely than M110I and Q113K mutations.

The VP4 ORF status differs among the mutants. tsD101 (Q113K) harbors the VP4 Gln 4 to Lys alteration, and tsD222 (M110I) harbors no VP4 ORF because of alteration in the initiation codon, whereas the tsD202 (P108S) VP4 ORF is unaffected by the mutation (Fig. 1). Chou and Martin (1974) showed that coinfection of

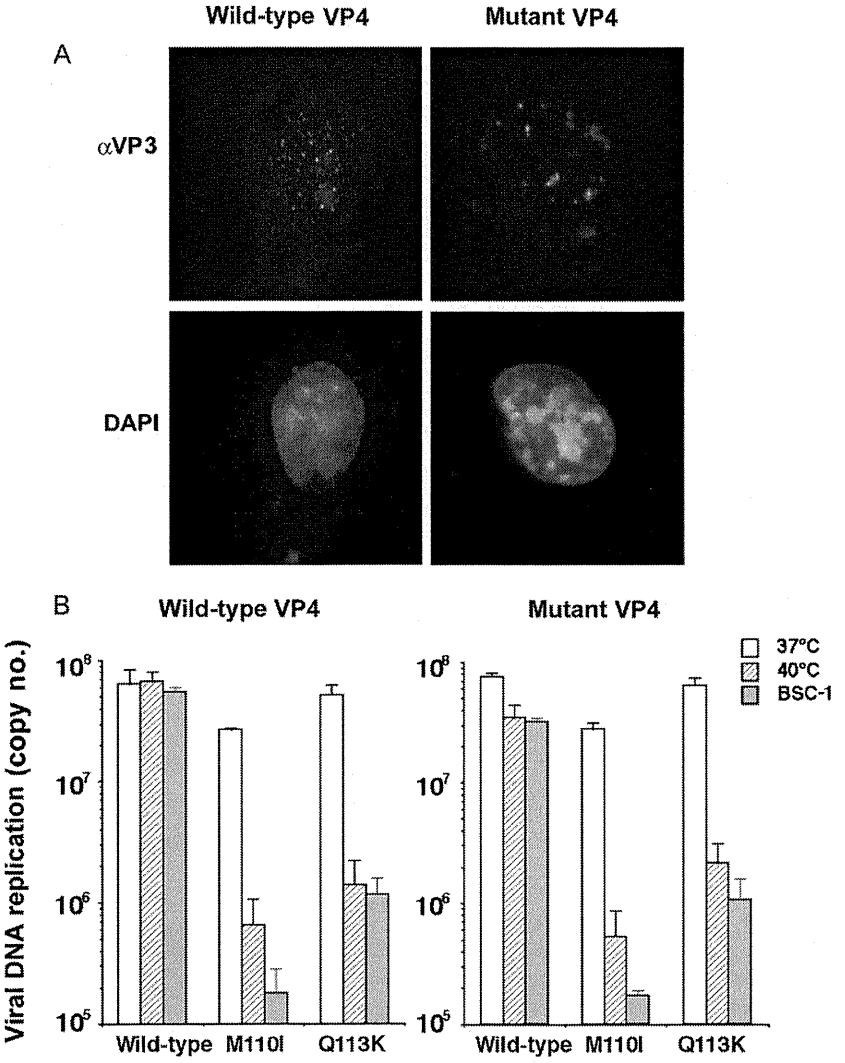

Fig. 3. VP4 complementation to mutant-infected cells. (A) Immunofluorescence detection of VP4 expressed from the VP4 expression vector: BSC-1 cells grown on coverslip were transfected with pSCMV VP4w or pSCMV VP4q using Lipofectamine 2000 (Invitrogen, Carlsbad, CA, USA) following the manufacturer's instruction. Cells were fixed at 48-h after transfection with acetone–methanol and stained for VP4 using rabbit anti-VP3 antibody (Abcam, Cambridge, UK) followed by Alexa Fluor 555-conjugated goat anti-rabbit IgG antibody (Molecular probes, Eugene, OR, USA). 4′,6-diamidino-2-phenylindole (DAPI) was used to counterstain for visualizing the cell nucleus. Identical set of cells showing representative images observed under the epifluorescent microscope are shown. (B) Viral DNA replication on VP4 complementation: CV-1 or BSC-1 cells grown in six-well plates were applied with approximately 1000 viral particles and approximately 1000 SV40 vectors carrying the VP4 expression vector to each cell. Viral DNA found in the cells coinfected with the vector carrying either pSCMV VP4w (left panel: Wild-type VP4) or pSCMV VP4q (right panel: Mutant VP4) incubated at designated temperature at 96 hpi was quantified for viral DNA as shown in Fig. 1B. The columns are marked as shown in Fig. 2B.

tsD202 and tsD222 or tsD101 at the non-permissive temperature did not complement the plaque forming-activity, showing that each pair of mutants harbor a genetically indistinguishable defect. Similarly, coinfection of CV-1 cells with Q113K and M110I with a natural SV40 backbone at 40 °C did not change their plaque-forming activity, confirming that the mutants belong to the same complementation group and their defects are genetically indistinguishable (Supplemental Table S1). When the mutations were combined, exemplified in the PMQ/SIK mutant, growth was more severely affected than those in the original mutants (Fig. 1B), suggesting that the gathered mutations had a cumulative impact on viral growth.

We examined by Western blot the presence or absence of VP4 in CV-1 and BSC-1 cells infected with their respective mutants. However, multiple attempts to detect VP4 using an antibody similar to that used in the original report (Daniels et al., 2007) (and provided by the same source) as well as a commercially available antibody (Anti-VP2/3; Abcam, Cambridge, UK) were unsuccessful. The VP3 proteins appeared to be highly prone to partial digestion in the cell, and proteins smaller than VP3 (approximately 25, 18, 16, and 12 kDa) that were reactive to the antibody were frequently detected in the virus-infected cells, causing difficulty in identifying the VP4 band (data not shown). We also examined VP4 ORF by *in vitro* translation using the PCR fragments harboring the VP3 coding region of either wild-type's or the mutants'. We did find VP4-like band, though very faint, that appeared in the *in vitro* translation of the wild-type VP3 coding region but not in those harboring M110I mutation (Supplemental Fig. S3). Instead of pursuing VP4 detection, we examined whether lack of VP4 is the cause of the growth defect at non-permissive temperatures in CV-1 cells or of the reduced infectivity in BSC-1 cells, i.e., whether supplying VP4 to mutant-infected cells would restore viral growth. To this end, we made the VP4 expression vectors pSCMV VP4w and pSCMV VP4q carrying wild-type VP4 ORF and VP4 ORF with VP3 Q113K (VP4 Q4K) mutation, respectively. Briefly, the ZsGreen coding region of pSCMV-ZG (Nakanishi

et al., 2008) was replaced with that of VP4 ORFs amplified by PCR using NOpSV40 or NOpSV40 Q113K as the template and the primers

5′-GGCCCGGGATCCACCGGTCGCCACCATGGTGAGACAAGTAGCC-3′

and 5′-TCTAGAGGGTCGTGTACATTAACTC-3′ (restriction sites are underlined) using the *AgeI* and *BsrGI* sites. The constructs harbor the human cytomegalovirus immediate-early promoter and SV40 origin that drives expression of VP4, introduced with a strong ATG context (boxed sequence in the primer) for ensuring VP4 translation, and are also available for packaging to the SV40 vector because of the presence of the SV40 origin (Nakanishi et al., 2008). On transfection of the constructs into BSC-1 cells followed by immunofluorescence detection of VP4 using anti-VP3 antibody, positive signals seen as nuclear dots, similar to those reported previously (Daniels et al., 2007), were evident (Fig. 3A). SV40 vectors packaging pSCMV VP4w or VP4q were then made by cotransfection of 293T cells with pCAG SV40, pCI Ts, and either pSCMV VP4w or VP4q, purified for the SV40 vector by 27–39% Optiprep gradient sedimentation (Nakanishi et al., 2008). The vectors were transduced into CV-1 or BSC-1 cells and coinfected with the viral particles either of wild-type, M110I, or Q113K. The cells were then examined for the extent of viral DNA replication at 96 hpi using quantitative real-time PCR (Fig. 3B). On coinfection with the VP4 vector expressing wild-type or mutant VP4, the extent of viral DNA replication did not recover in mutant-infected CV-1 cells incubated at non-permissive temperature as well as in mutant-infected BSC-1 cells; the profile of viral growth defect was unchanged with or without wild-type VP4 transduction by the VP4 expression vector. The results suggested that presence of wild-type or mutant VP4 did not complement the growth defect of the mutants and was consistent with the idea that these growth defects occur in the early stages of infection.

Here we report that the tsD222 mutant is identical to VP2 M228I, known to be defective in expressing VP4 (Daniels et al., 2007), though the mutant showed a conditional temperature growth phenotype in CV-1 cells. Genetic complementation studies confirmed that the growth defect was not related to the absence of an intact VP4 ORF, since the growth of tsD101 (Q113K), in which VP4's fourth amino acid was altered from Gln to Lys, and tsD202 (P108S), in which VP4 ORF was intact, was also affected, and they did not genetically complement each other. The mutants in the context of a natural genome as well as in the context of an NOSV40 viral genome, in which the overlapping coding regions of VP2/3 and VP1 are separated by a duplication of the overlapping region, exhibited similar phenotypes with a temperature-sensitive growth defect in CV-1 cells and the inability to genetically complement each other (Supplemental Table S1 and data not shown). Consistent with these results, supplying VP4 *in trans* using the VP4 expression vector did not ameliorate the mutants' growth at non-permissive temperatures and in BSC-1 cells (Fig. 3). Since viral gene expression and DNA replication were affected by the mutations, our results indicated that the defect in the mutants involves one or more defects in VP2/3. This is reasonable given that VP4 is a nonstructural protein that is expressed in the very late stage of infection and thus mediating viral spread, which is the major role of VP4 (Daniels et al., 2007). Thus, the effect of tsD mutation is more significant in the early stages of viral infection during viral propagation, and a defect in mutant VP2/3 made a more significant contribution to the temperature-sensitive phenotype than the absence of a functional VP4.

Acknowledgments

We thank Dr. Ariella Oppenheim (Hebrew University) for the generous gift of anti-VP3 anti-serum, and Dr. Harumi Kasamatsu (University of California, Los Angeles) and Dr. Mary J. Tevethia (Pennsylvania State University) for providing the viral lysates of tsD101, tsD202, and tsD222. This work was supported by a Grant-in-Aid for Scientific Research from Japan Society for the Promotion of Science and Health Labor Sciences Research Grant on "Research on Emerging and Re-emerging Infectious Diseases" to AN.

Appendix A. Supplementary data

Supplementary data associated with this article can be found, in the online version, at doi:10.1016/j.virusres.2011.02.001.

References

Avila, J., Saral, R., Martin, R.G., Khoury, G., 1976. The temperature-sensitive defect in SV40 group D mutants. Virology 73 (1), 89–95.
Chen, X.S., Stehle, T., Harrison, S.C., 1998. Interaction of polyomavirus internal protein VP2 with the major capsid protein VP1 and implications for participation of VP2 in viral entry. EMBO J. 17 (12), 3233–3240.
Chou, J.Y., Avila, J., Martin, R.G., 1974. Viral DNA synthesis in cells infected by temperature-sensitive mutants of simian virus 40. J. Virol. 14 (1), 116–124.
Chou, J.Y., Martin, R.G., 1974. Complementation analysis of simian virus 40 mutants. J. Virol. 13 (5), 1101–1109.
Chou, J.Y., Martin, R.G., 1975. DNA infectivity and the induction of host DNA synthesis with temperature-sensitive mutants of simian virus 40. J. Virol. 15 (1), 145–150.
Daniels, R., Sadowicz, D., Hebert, D.N., 2007. A very late viral protein triggers the lytic release of SV40. PLoS Pathog. 3 (7), e98.
Ishii, N., Nakanishi, A., Yamada, M., Macalalad, M.H., Kasamatsu, H., 1994. Functional complementation of nuclear targeting-defective mutants of simian virus 40 structural proteins. J. Virol. 68 (12), 8209–8216.
Lai, C.J., Nathans, D., 1975a. A map of temperature-sensitive mutants of simian virus 40. Virology 66 (1), 70–81.
Lai, C.J., Nathans, D., 1975b. Mapping the genes of simian virus 40. Cold. Spring. Harb. Sympos. Quant. Biol. 39 (Pt. 1), 53–60.
Li, P.P., Naknanishi, A., Tran, M.A., Ishizu, K., Kawano, M., Phillips, M., Handa, H., Liddington, R.C., Kasamatsu, H., 2003. Importance of Vp1 calcium-binding residues in assembly, cell entry, and nuclear entry of simian virus 40. J. Virol. 77 (13), 7527–7538.
Nakanishi, A., Chapellier, B., Maekawa, N., Hiramoto, M., Kuge, T., Takahashi, R.U., Handa, H., Imai, T., 2008. SV40 vectors carrying minimal sequence of viral origin with exchangeable capsids. Virology 379 (1), 110–117.
Nakanishi, A., Nakamura, A., Liddington, R., Kasamatsu, H., 2006. Identification of amino acid residues within simian virus 40 capsid proteins Vp1, Vp2, and Vp3 that are required for their interaction and for viral infection. J. Virol. 80 (18), 8891–8898.
Nakanishi, A., Shum, D., Morioka, H., Otsuka, E., Kasamatsu, H., 2002. Interaction of the Vp3 nuclear localization signal with the importin alpha 2/beta heterodimer directs nuclear entry of infecting simian virus 40. J. Virol. 76 (18), 9368–9377.
Reddy, V.B., Thimmappaya, B., Dhar, R., Subramanian, K.N., Zain, B.S., Pan, J., Ghosh, P.K., Celma, M.L., Weissman, S.M., 1978. The genome of simian virus 40. Science 200 (4341), 494–502.
Ritzi, E., Levine, A.J., 1970. Deoxyribonucleic acid replication in simian virus 40-infected cells. III. Comparison of simian virus 40 lytic infection in three different monkey kidney cell lines. J. Virol. 5 (6), 686–692.
Robb, J.A., Martin, R.G., 1972. Genetic analysis of simian virus 40.3. Characterization of a temperature-sensitive mutant blocked at an early stage of productive infection in monkey cells. J. Virol. 9 (6), 956–968.
Shenk, T.E., Rhodes, C., Rigby, P.W., Berg, P., 1975. Mapping of mutational alterations in DNA with S1 nuclease: the location of deletions, insertions and temperature-sensitive mutations in SV40. Cold. Spring. Harb. Symp. Quant. Biol. 39 (Pt. 1), 61–67.

Virology 412 (2011) 179–187

Contents lists available at ScienceDirect

Virology

journal homepage: www.elsevier.com/locate/yviro

Novel DNA virus isolated from samples showing endothelial cell necrosis in the Japanese eel, *Anguilla japonica*

Tetsuya Mizutani [a,*,1], Yusuke Sayama [a,b,1], Akira Nakanishi [c,1], Hideharu Ochiai [d], Kouji Sakai [e], Kouji Wakabayashi [f,2], Nozomi Tanaka [f], Emi Miura [f], Mami Oba [a], Ichiro Kurane [a], Masayuki Saijo [a], Shigeru Morikawa [a], Shin-ichi Ono [f,*]

[a] *Virology 1, National Institute of Infectious Diseases, Gakuen 4-7-1, Musashimurayama, Tokyo 208-0011, Japan*
[b] *Department of Virology, Tohoku University School of Medicine, 2-1 Seiryo-machi, Aoba-ku, Sendai 980-8575, Japan*
[c] *National Center for Geriatrics and Gerontology, 35 Gengo, Morioka-machi, Obu, Aichi 474-8522, Japan*
[d] *Research Institute of Biosciences, Azabu University, Fuchinobe 1-17-71, Chuo-ku, Sagamihara, Kanagawa 252-5201, Japan*
[e] *Division of Experimental Animals Research, National Institute of Infectious Diseases, 4-7-1 Gakuen, Musashi-Murayama, Tokyo 208-0011, Japan*
[f] *School of Marine Science and Technology, Tokai University, 3-20-1 Orido, Shimizu-ku, Shizuoka 424-8610, Japan*

ARTICLE INFO

Article history:
Received 19 October 2010
Returned to author for revision
6 December 2010
Accepted 28 December 2010
Available online 1 February 2011

Keywords:
Novel DNA virus
Japanese eel endothelial cells-infecting virus
Anguilla japonica

ABSTRACT

Economic loss due to viral endothelial cell necrosis of eel (VECNE) of *Anguilla japonica* is a serious problem for the cultured Japanese eel market. However, the viral genome responsible for VECNE is unknown. We recently developed a rapid determination system for viral nucleic acid sequences (RDV) to determine viral genome sequences. In this study, viral DNA fragments were obtained using RDV, and approximately 15-kbp circular full genome sequences were determined using a next-generation sequencing system, overlapping PCR, and Southern blot analysis. One open reading frame (ORF) was homologous to the large T-antigen of polyomavirus; other ORFs have no homology with any nucleic or amino acid sequences of polyomavirus. Therefore, as this DNA virus might comprise a novel virus family, we provisionally named it Japanese eel endothelial cells-infecting virus (JEECV). JEECV was detected in both naturally and experimentally infected eels, suggesting that JEECV potentially causes VECNE.

Introduction

The Japanese eel *Anguilla japonica* is an important fish species in several Asian countries including Japan. Viral endothelial cell necrosis of eel (VECNE) of *A. japonica* is a serious problem in Japanese aquaculture industry (Egusa et al, 1989; Inoue et al, 1994; Ono and Nagai, 1997). In Shizuoka, a prefecture where the eel is mass-produced, the total production of Japanese eel was approximately 1700 tons (4 billion yen), and 107 tons worth of eel died from illness in 2008. Of these 107, 31 tons worth of the eels died from VECNE. Thus, economic loss due to VECNE is a serious problem in the cultured eel business. To prevent the spread of VECNE, obtaining genomic information of the unknown viral agent is crucial for developing a detection system and vaccines.

We and other groups reported that VECNE occurs naturally (Egusa et al, 1989; Inoue et al, 1994; Ono and Nagai, 1997). Naturally VECNE shows reddening of fins with a swollen abdomen. Intense congestion occurs in the gills, liver, and intestine. Histopathology of VECNE is characterized by intense congestion in the central venous sinuses of the gill filaments compared to healthy eels. This pathological change is accompanied by degeneration of nuclei of endothelial cell in blood vessels; this degeneration is characterized by swelling. Hexagonal virus particles measuring about 75 nm in diameter were observed in the nuclei. Thus, VECNE results from a systemic viral infection that causes necrosis of endothelial cells in blood vessels. VECNE was experimentally induced by injecting a filtered homogenized solution of diseased eels into the abdominal cavities of healthy eels (Ono and Nagai, 1997). Since the first report regarding VECNE was published in 1989 (Egusa et al, 1989), the causative virus has not been identified because cell culture systems for viral isolation are not available. Therefore, we established a cell line that originated from vascular endothelial cells of *A. japonica* (Ono et al, 2007). The primary Japanese eel endothelial (JEE) cell culture system was established using the dorsal aorta and aortic bulbs of healthy eels. To isolate the causative virus, gill lamellae were homogenized and centrifuged. The supernatant was then filtered using a 0.45-μm filter. The filtrate was added to JEE cells. At 7 days post-inoculation (p.i.), cytopathic effect (CPE) with markedly hypertrophied nuclei was observed (Ono et al, 2007). After a second passage, CPE was observed at 4 days p.i. Serial passages of the virus in JEE cells also induced CPE. When JEE cells were treated with 5-iodo-2′-deoxyuridine before virus inoculation, CPE was inhibited, strongly suggesting that the virus has DNA as its genome. In addition, this virus exhibited chloroform

* Corresponding authors. T. Mizutani is to be contacted at Fax: +81 425 65 3315.
E-mail address: tmizutan@nih.go.jp (T. Mizutani).
[1] These authors contributed equally to this study.
[2] Present address: International Pet World College, Niigata, 950-0911, Japan.

0042-6822/$ – see front matter © 2011 Elsevier Inc. All rights reserved.
doi:10.1016/j.virol.2010.12.057

resistance, suggesting it is not an envelope virus. The shape of this virus in JEE cells is the same as that in naturally infected eels, as confirmed by electron microscopy (EM). The isolated virus caused VECNE in eels, as determined by a previous study (Ono et al, 2007). Although this virus was believed to be an adenovirus-like virus from these data, nucleic acid sequences were not determined.

We recently developed a rapid determination system for viral nucleic acid sequences (called RDV) to determine viral genomic sequences without cloning in a plasmid vector (Mizutani et al, 2007). RDV allows for exhaustive identification of viruses compared to previous virus detection systems, such as RT-PCR, because it does not require specific primers for target virus nucleotide sequences. In previous studies, we identified several novel viruses, such as Ryukyu virus 1 (bat adenovirus) (Maeda et al, 2008), *Hipposideros diadema* herpesvirus 1 (from bat) (Watanabe et al, 2009), Bat betaherpesvirus 2 (Watanabe et al., in press), Ostrich virus 1 (orthoreovirus) (Sakai et al, 2009) and Phasi Charoen virus (mosquito bunyavirus) (Yamao et al, 2009). In this study, we used RDV with the supernatant of virus-infected JEE cells to obtain viral genomic sequences of the viruses infecting JEE cells.

Results

Virus shape in virus stock analyzed using EM

To confirm that the virus stocks (supernatant of virus-infected cells) cause VECNE in eels, 70th-passage virus stock was used in this study. Virus shapes were observed in the nuclei using electron microscopy (EM) (Fig. 1A and B) after JEE cells were infected with the virus stock. After filtering the virus stock using 0.45-μm filters, the virus was inoculated into eels. EM photographs of the gill are illustrated in Fig. 1C and D. Intense congestion occurred in the gill (Fig. 1E) and liver (Fig. 1F) at 8 days p.i. Although we evaluated a number of EM photographs of JEE cells and gills, we found only one species based on virus shape. This suggests that the virus stock over 70 passages in JEE cells contain agent(s) causing VECNE.

Partial viral genomic DNA sequences using RDV

To obtain viral DNA genomic sequences, DNA was extracted from the supernatant of virus-infected JEE cells at 4 days p.i. after RNase A and DNase I treatment. RDV was then performed. A total of 29 PCR products were extracted from agarose gels at the final step of RDV, and direct sequencing was performed. The nucleotide sequences were used to determine homologous sequences using BLASTx and tBLAST at the National Center for Biotechnology Information (NCBI) web site. Nine read sequences were not homologous to any genes. PCR primers were designed based on these sequences, and three read sequences (read-024, -004A, and -004C) were amplified in virus-infected cells, but not in mock-infected cells, using DNA samples (Fig. 2A). One read sequence, read-024, comprising 100 amino acids were homologous to the sequence of the large T-antigen of polyomaviruses, such as budgerigar fledgling disease virus and human polyomaviruses. Read-024 was detected using RT-PCR using the RNA extracted from virus-infected cells at 3 days p.i. (Fig. 2B), indicating that it was transcribed in infected cells. In addition, 16S ribosomal DNA of bacteria and mycoplasma was not detected in these DNA samples using PCR (data not shown). These results indicated that these read sequences obtained using RDV were parts of the viral genome.

Elongation of viral genomic sequences

Based on these viral nucleotide sequences, genome walking was performed using differential display RT-PCR (GeneFishing DEG Premix Kit; Seegene). We obtained DNA fragments of 5 and 2 kbp approximately. To obtain the entire genome sequence of this virus, we used the Genome Sequencer FLX System (Titanium) of Roche and 454 Life Sciences. Viral DNA was extracted by precipitation of 30-ml virus-infected cell supernatant at 4 days p.i using ultracentrifugation. The obtained 17,000 read sequences were analyzed using the GS *De novo* Assembler Version 2.3 (Roche) for *de novo* assembly. As a result, we obtained 15,131 total nucleotides with circular DNA forms comprising this viral genome (Fig. 3A). The viral genomic information was deposited in DDBJ/EMBL/GenBank (accession number AB543063). Organization of the viral genome is illustrated in Fig. 3B. Because we could not find a motif of replicative origin on this genome, the provisional nucleotide number is 1 in Fig. 3A and B. The locations of partial DNA fragments (read-024, -004A, and -004C) obtained using RDV and two long DNA fragments (5 and 2 kbp) obtained using genome walking are also illustrated in Fig. 3B. In addition, at least 15 predicted ORFs were found in both strands using GeneMark.hmm 2.0 (Fig. 3B). These ORFs, except for the large T-antigen-like ORFs, are not homologous to any genes of polyomavirus.

Regions homologous to polyomaviruses

The DNA sequence harbored an ORF encoding 698 amino acids; a region of this reading frame contains approximately 100 amino acids as determined using RDV. This ORF is homologous to the large T-antigen gene of avian polyomaviruses at ATP-binding region (E value of 8e-54) (Fig. 4A and B), although it is distinct from the usual configuration of polyomaviral T-antigen genes. Usually, T-antigen genes carry an intron in the middle of the sequence having one splice donor and two splicing acceptors, allowing alternative splicing to produce mRNA for large and small T-antigens. In contrast, the ORF appeared contiguous without introns, suggesting that the DNA is not a direct descendent of a polyomaviral DNA and likely belongs to a novel virus family. We provisionally named this DNA as JEE cells-infecting virus (JEECV).

Multiplicity of JEECV in JEE cells

To investigate multiplicity of JEECV in JEE cells, a TaqMan real-time PCR system was developed. Probe and primers were designed for the large T-antigen-like region. The virus stock at 0.01 $TCID_{50}$/cell multiplicity of infection (MOI) was inoculated into confluent JEE cells in a 24-well plate, and cells and supernatant were harvested at 24, 48, 72, 96, 120, 144, 163, and 187 h p.i. As illustrated in Fig. 5A, viral gene numbers increased in the cells and supernatant from 24 to 144 h p.i. Conventional PCR was also performed, and similar results were obtained (Fig. 5B).

Demonstration of intact genome size of JEECV

As illustrated in Fig. 3, 454 analysis revealed that JEECV genome is circular. We then performed rolling circle analysis for amplifying circular viral genomes (Johne, 2009). DNA extracted from the supernatant of virus-infected cells at 163 h p.i. (Fig. 4) was amplified using Phi29 enzymes (Templiphi) for circular DNA, and viral copy numbers were calculated for amplified products using real-time PCR (Fig. 4A). As a result, products of Templiphi were amplified approximately 128-fold compared with unamplified DNA (data not shown).

The reads using the next-generation sequencer were obtained as contiguous sequences (data not shown). To confirm that the circular viral genome exists, overlapping PCR on the viral genome was performed. DNA extracted from JEECV-infected cells was amplified using long PCR by overlapping the amplified region. As illustrated in Fig. 6A, we obtained PCR products at expected sizes. We confirmed the nucleotide sequences of bands after gel purification. This result suggests the presence of a circular viral genome in infected cells. In the viral genomic sequence, a repeat region is observed at 480–853 nt. The repeat region was sequenced within the long PCR product. Although we deposited a viral genomic sequence with three repeats in

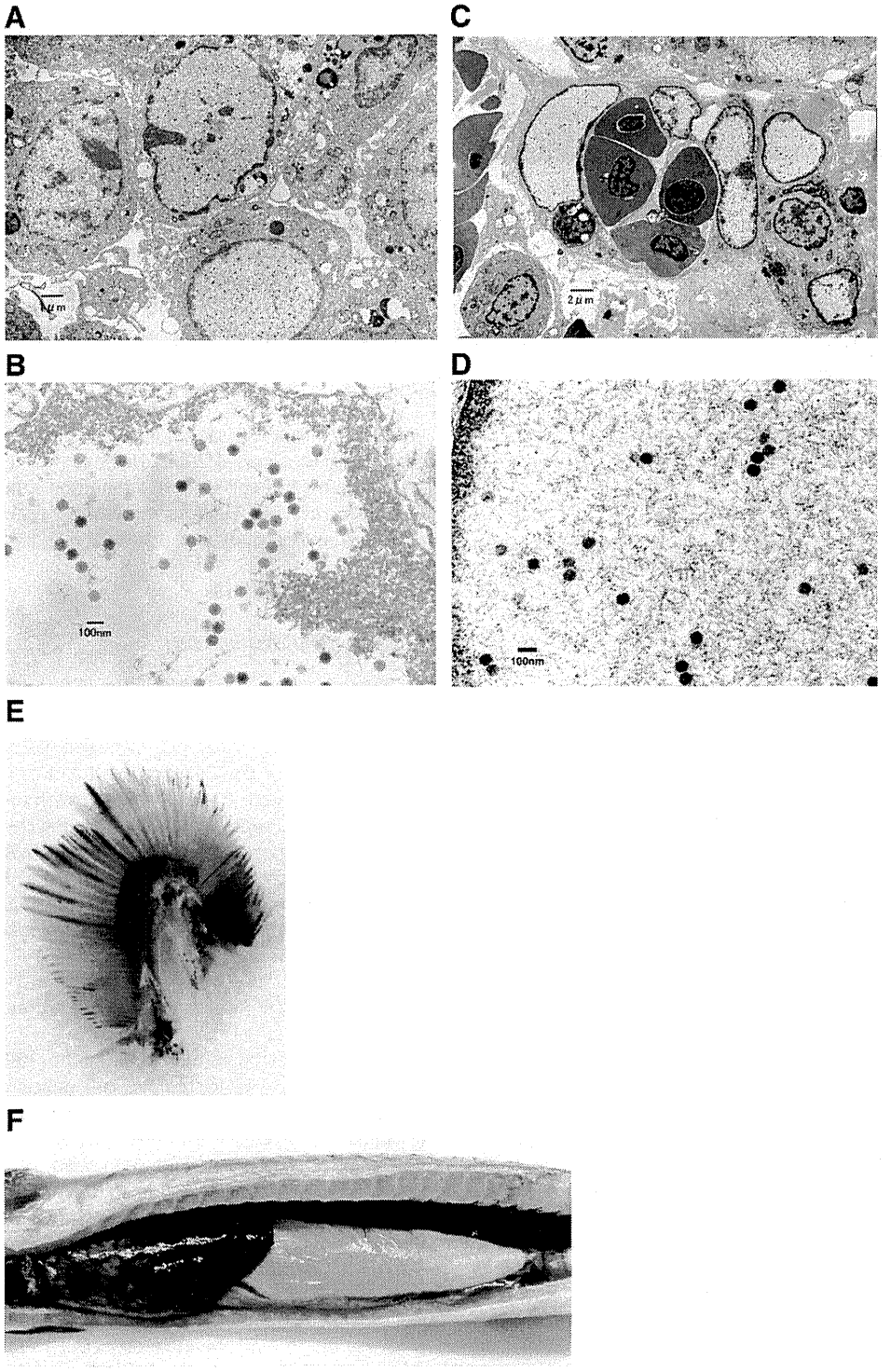

Fig. 1. Virus passage in JEE cells and infection in eels. 70th passage virus stock was infected to JEE cells (A and B) and healthy eel (C and D). EM photographs of B and D illustrate the enlarged images of A and C, respectively. Panels E and F illustrate gills and livers of virus-infected eel, respectively.

GenBank, we also detected two repeats using PCR (data not shown). Therefore, there should be different repeat numbers in virus-infected cells.

To further confirm the genomic DNA size of JEECV, we performed Southern blot analysis. DNA was digested using the restriction enzyme *BglII*, which is expected to induce a single cut in the viral genome at a position of 14418 nt. As indicated in Fig. 6B, a single band was found at approximately 15 kbp for *BglII*-digested DNA. Further confirmation is required with regard to the appropriate size for such large molecules of DNA. Another large-size DNA from nondigested DNA was observed after long exposure of the X-ray film. This band may represent another form of JEECV.

Detection of JEECV in eels

To confirm the infection of eels with JEECV, DNA was extracted from the gills of eels with natural VECNE and used to experimentally infect eels. PCR was performed for amplifying three different regions

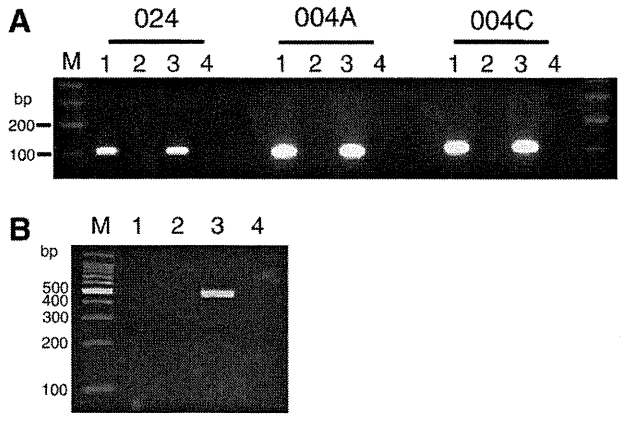

Fig. 2. Determination of viral genome sequence. A. Detection of viral DNA fragments. Three unknown DNA fragments (004A, 004C, and 024) are obtained using RDV. Primers are designed (004A-1 and -2, 004C-1 and -2, 024-3 and -4), and PCR is performed using the supernatant of virus-infected cultured cells at 7 days p.i. M, 100-bp DNA ladder marker; lane 1, supernatant of JEECV-infected cells; lane 2, supernatant of mock-infected cells; lane 3, JEECV-infected cells; lane 4, mock-infected cells. B. Detection of viral transcript. RT-PCR is performed using RNA extracted from virus-infected cells at 3 days p.i. to detect viral transcripts of the region harboring read-024 using PCR primers, 024-2 and 024-5. M, 100-bp DNA ladder marker; lanes 1 and 2, mock-infected cells; and lanes 3 and 4, JEECV-infected cells. Reaction of cDNA synthesis in lanes 2 and 4 is performed without Superscript III enzyme.

of viral genome. As illustrated in Fig. 7, viral genes were amplified in eels with natural VECNE and virus-infected eels, but not in healthy eels. Nucleotide sequences of these PCR products were confirmed after gel purification.

Discussion

In this study, we determined the genomic sequence of a novel eel virus, JEECV, which was isolated from eels with VECNE. The virus stock used in this study contained agent(s) that cause VECNE. Our results from 454 analysis, rolling circle amplification, and overlapping PCR suggested that JEECV genome is circular. We could not determine whether linear form exists in this study. Therefore, we believe that JEECV genome has two forms, linear and circular, in virus-infected cells. In addition, it is also possible that the entire linear form of the viral genome is longer than the present length obtained using Southern blot analysis. Viral genomic sequences in this study may represent one form of JEECV.

Interestingly, JEECV DNA contains regions homologous to the large T-antigen gene of polyomaviruses at ATP binding region, suggesting that this homologous region has biological function. We also investigated that bird polyomaviral T-antigen genes were more homologous to JEECV than mammals. Among four currently known bird polyomaviruses, avian polyomavirus, goose hemorrhagic polyomavirus (GHPV), finch polyomavirus, and crow polyomavirus (John and Muller, 2007), the diseases caused by GHPV (hemorrhagic nephritis and enteritis) resemble VECNE. JEECV large T antigen-like region also contains motifs conserved among polyomavirus T-antigens: DNAJ (HPDK) motif, the canonical nuclear localization signal, and zinc finger motif. Conserved region 1 (CR1) motif was found in the C-terminus, instead of N-terminus where commonly found in the polyomaviral T-antigen (Pipas, 1992). It remains to be examined whether the T-antigen-like gene influences VECNE disease symptoms, as the T-antigen genes of polyomaviruses are known to be tumorigenic. We found that the transcript harboring the large T-antigen-like gene region was detectable, thus it is possible that the T-antigen gene product is expressed. Further investigation is needed to identify the structural and nonstructural viral protein ORFs in JEECV DNA and to determine the role of viral proteins, including the T-antigen-like gene, in the development of VECNE *in vivo*.

Recently, two novel viruses, bandicoot papillomatosis carcinomatosis virus (BPCV) 1 and 2, were detected from bandicoot (Bennett et al., 2008; Woolford et al., 2007, 2008 and 2009). These virus genomes have both T-antigens of an ancestral polyomavirus and the L1 and L2 capsid proteins of an ancestral papillomavirus. Inter-familial recombination was occurred between an ancient papillomavirus and an ancient polyomavirus more than 10 million years ago (Bennett et al., 2010). JEECV genome may also arise by recombination between a polyomavirus and a virus from unknown virus family.

We are also keen to investigate in the possibility of latent infection by JEECV in Japanese eels. Natural VECNE is occasionally observed in kidneys or liver without symptoms in gills (data not shown). It is difficult to locate diseased eels exhibiting such weak symptoms. Therefore, we believe that there are eels latently infected by JEECV exhibiting very weak symptoms.

In a previous study, mortality after viral infection was reduced by incubating infected eels for more than 3 days at 35 °C under nonfeeding conditions (Tanaka et al, 2008). However, it is not cost-effective to treat a great number of eels with this condition simultaneously. To prevent the prevalence of VECNE, a monitoring system for JEECV infection developed in this study may be useful, if JEECV indeed causes VECNE.

Materials and methods

Cells, virus and viral infection

JEE cells were cultured in a medium containing Humedia-EB2 (Kurabo, Japan) and EGM-2 (Lonza, Switzerland) on a gelatin-coated 6-cm dish at 25 °C in a 5% CO_2 incubator. JEE cells were infected with the virus stock at 0.01 $TCID_{50}$/cell MOI. At 4 or 5 days p.i., the infectious fluid was harvested. To infect the eels with the virus experimentally, 1×10^6 $TCID_{50}$ (supernatant of virus-infected cultured cells) was inoculated intraperitoneally into healthy eels. At 10 days p.i., eels were analyzed. Tissues were homogenized using BioMasher (Wako Bio. Japan), and DNA was extracted using a QIAamp DNA mini kit. The experiments using eels were performed according to the regulations of Tokai University.

Analysis using RDV (Maeda et al., 2008; Mizutani et al., 2007)

The viral infected culture supernatant (100 μl) was centrifuged at 2000*g*, 15 min, 4 °C to remove cell debris and was treated with 0.0001 μg RNase A (Qiagen), and 10-μl Turbo DNA-free DNase I (Applied Biosystems, USA) were mixed with 1× Turbo DNA-free buffer and shaken at 37 °C for 30 min. For DNA extraction, a QIAamp DNA mini kit was used according to the manufacturer's instructions. A whole-genome amplification system (WGA; Sigma-Aldrich, USA) was used according to the manufacturer's instructions. In the RDV method, AmpliTaq Gold LD (Applied Biosystems) was used to obtain a high yield of the PCR products. We mixed 4 μl 10× amplification buffer in a GenomePlex Whole Genome amplification kit (WGA1) (containing primers, but no information on sequences) containing 5-μl DNA solution, 0.25 μl AmpliTaq Gold LD, and 30.75 μl distilled water. The reaction mixture was heated at 95 °C for 9 min (for activation of AmpliTaq Gold), followed by 70 cycles of amplification consisting of an annealing step at 68 °C for 1 min, a primer extension step at 72 °C for 5 min, and a denaturation step at 94 °C for 1 min. After the first DNA library was purified using the MonoFas DNA isolation system (GL Science, Japan), DNA was digested with 40-U *Hae*III (Takara Bio Inc.) at 37 °C for 30 min, and then the digested DNA was purified using MonoFas. To construct the second cDNA library, 2.50 μl DNA solution, 0.5 μl blunt *EcoR*I–*Not*I–*Bam*HI adapter (Takara Bio Inc.), and 3 μl ligation mix (Takara Bio Inc.) were reacted at room temperature for 30 min, and then the digested DNA was isolated using MonoFas. The second cDNA library was amplified using PCR using specially designed primer sets in which six nucleotides comprised CC (*Hae*III-digested

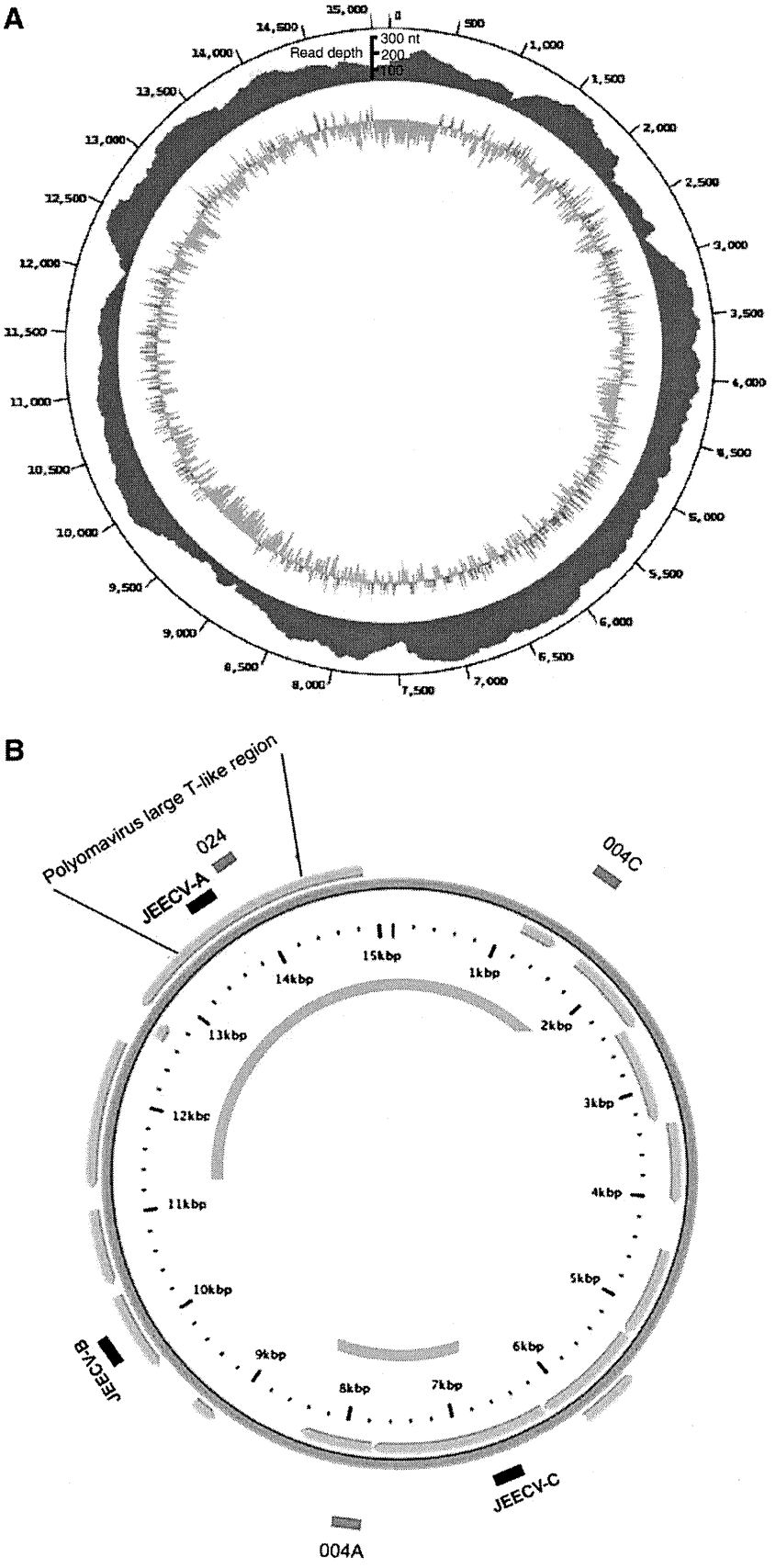

Fig. 3. Organization of the viral genome. (A) The cover depth of nucleotides analyzed using the next-generation sequencer is indicated in blue outside the JEECV genome. GC content is indicated inside the JEECV genome. Red bar, more than 50% GC content in every 10 nucleotides; green bar, less than 50% GC content. (B) Fifteen predicted ORFs are indicated with arrows. Read DNA fragments obtained using RDV and genome walking DNA fragments are indicated as blue and green lines, respectively. Black lines indicate amplified regions by PCR in Fig. 7.

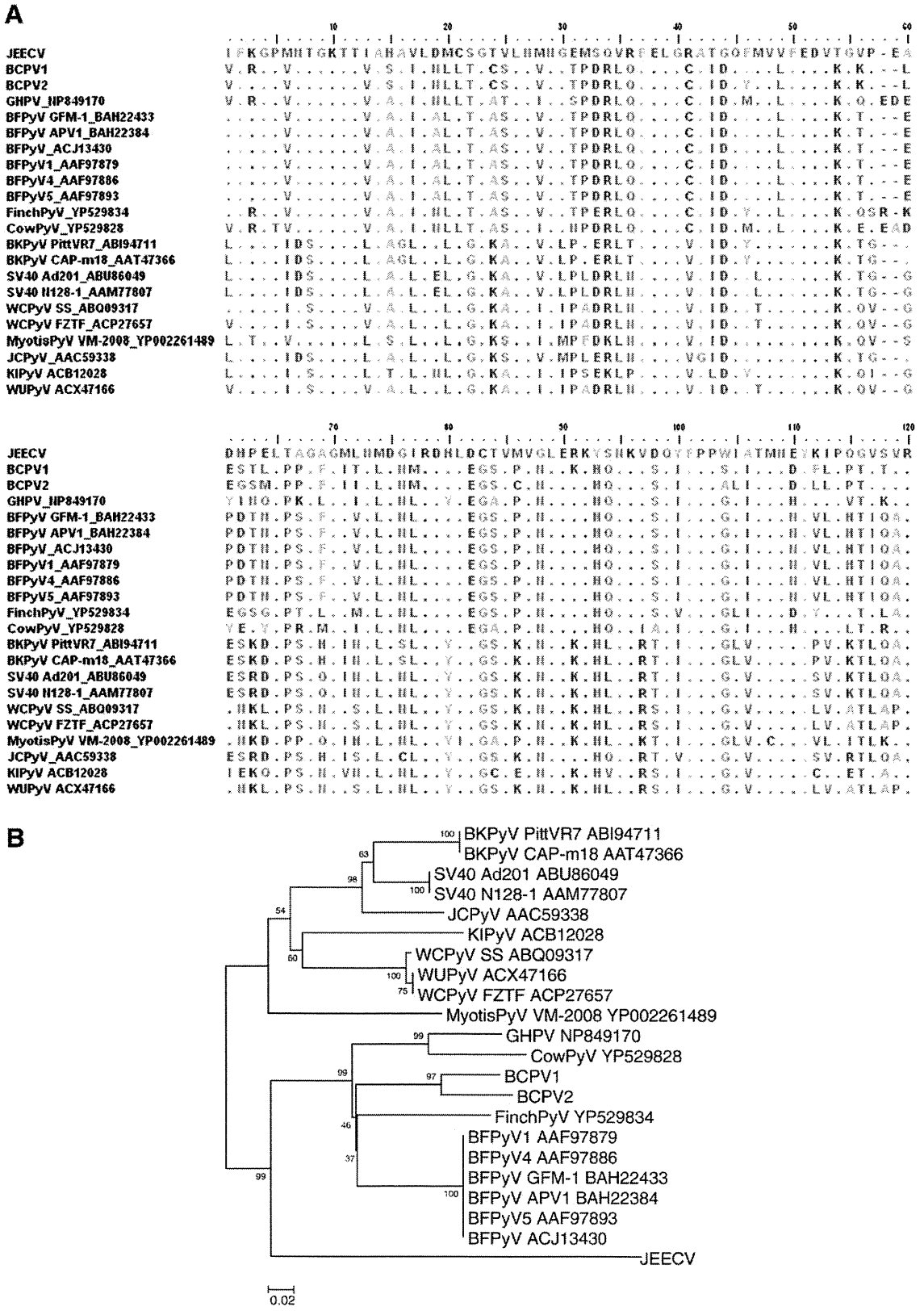

Fig. 4. Alignment of the large T-antigen-like protein. (A) Polyomavirus large T-antigen-like region of JEECV is compared with that of polyomaviruses deposited in GenBank. Alignment is performed using MEGA4 software. (B) Phylogenetic tree analysis of JEECV. The phylogenetic tree is obtained using the neighbor-joining method with 1000 bootstrap replicates, and branch length is indicated at each branch node. The horizontal scale indicates 0.02 amino acid substitutions per site. BCPV1 and 2, bandicoot papillomatosis carcinomatosis virus 1 and 2; GHPV, goose polyomavirus; BFPyV, budgerigar fledgling disease polyomavirus; finch PyV, finch polyomavirus; cow PyV, crow polyomavirus; BKPyV, BK polyomavirus; SV40, simian virus 40; WCPyV, WU polyomavirus; mytosis PyV, mytosis polyomavirus; and JCPyV, JC polyomavirus.

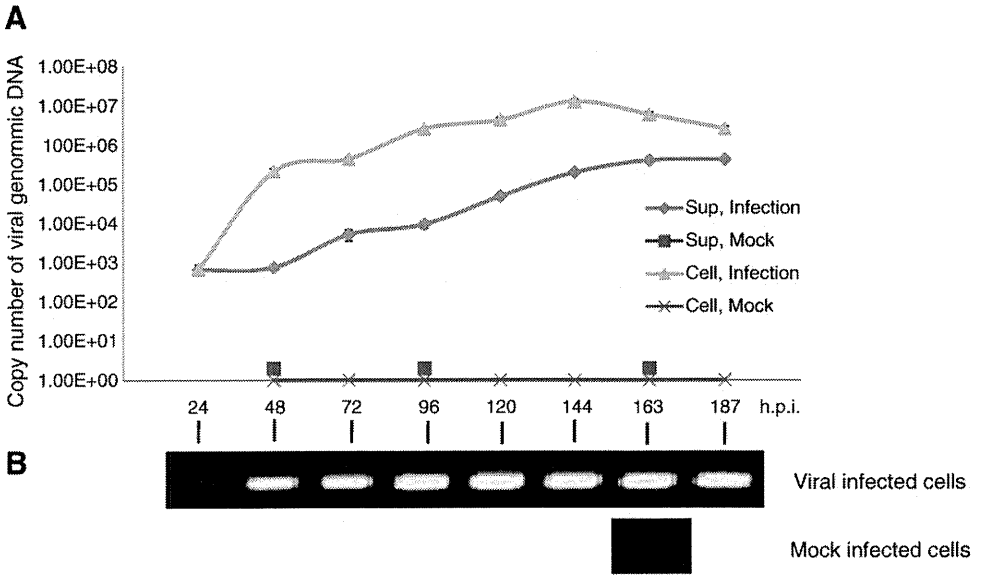

Fig. 5. Analysis of virus multiplication in JEE cells. JEECV (0.01 MOI) is infected into JEE cells. DNA extracted from cells and culture supernatant from 24 to 187 h p.i. is analyzed using real-time TaqMan PCR (A) and conventional PCR using primers, 024-3 and -4 (B).

sequence), and four variable nucleotides were added to the 3′ end of the adapter sequence. PCR was performed by mixing 15 μl AmpliTaq Gold PCR Master Mix containing AmpliTaq Gold, 0.5 μl forward primer, 0.5 μl reverse primer, 0.5 μl DNA solution, and 13.5 μl distilled water. The reaction mixture was heated at 95 °C for 12 min, followed by 70 cycles of amplification consisting of annealing and primer extension at 72 °C for 30 s and denaturation at 94 °C for 30 s. After electrophoresis of PCR products, DNA was isolated from the gel using MonoFas. Direct sequencing was performed using the forward primer and/or reverse primer.

Conventional PCR

For PCR, DNA and RNA were extracted from the supernatant and cells using the QIAamp DNA mini kit (Qiagen, USA). In this study, we used GoTaq Master Mix (Promega, USA) for conventional PCR. The

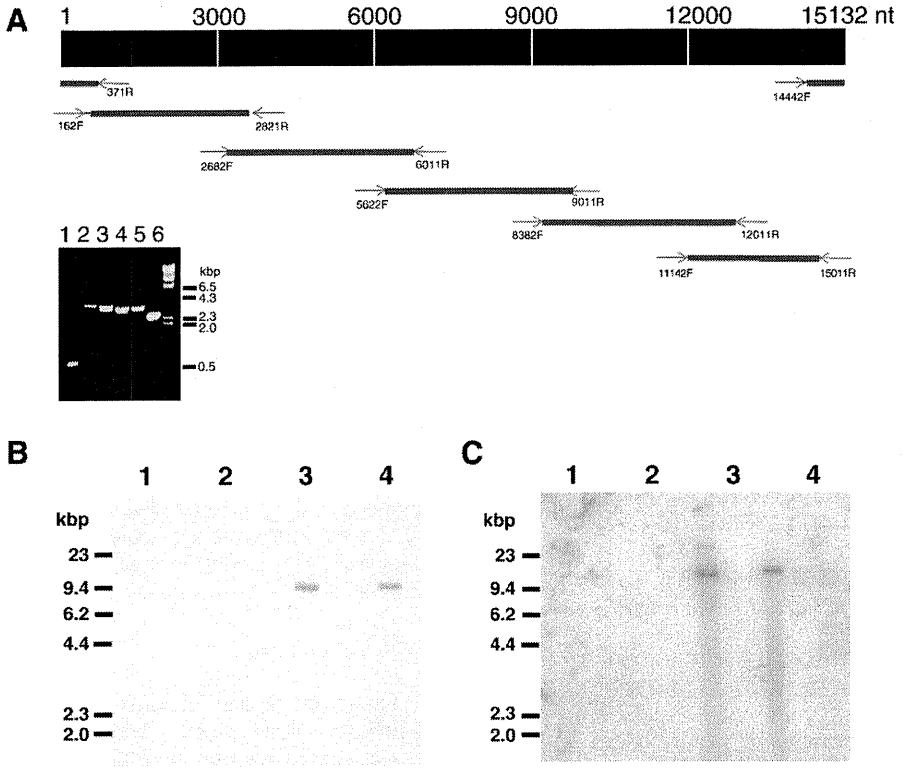

Fig. 6. Circular form of JEECV. (A) Overlapping PCR. Lane 1, 14442F and 371R primers; lane 2, 11142F and 15011R primers; lane 3, 8382F and 12011R; lane 4, 5622F and 9011R primers; lane 5, 2682F and 6011R primers; lane 6, 162F and 2821R primers. (B) Southern blot analysis with short exposure of X-ray film. (C) Southern blot analysis with long exposure using Image analyzer. Lane 1, no digested DNA from mock-infected cells; lane 2, *BglII*-digested DNA from mock-infected cells; and lane 3, no digested DNA from JJECV-infected cells; lane 4, *BglII*-digested DNA from JEECV-infected cells.

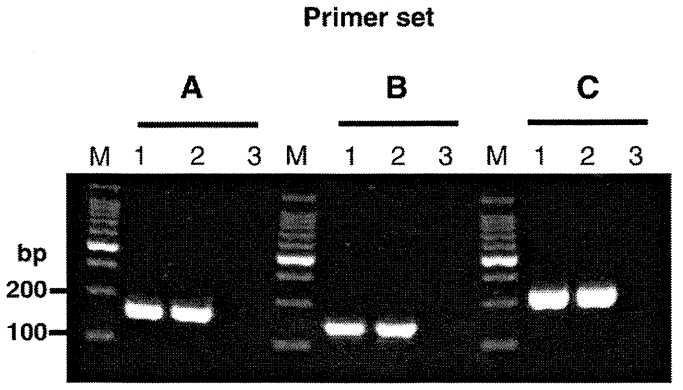

Fig. 7. Detection of JEECV in eels. Healthy eels are inoculated intraperitoneally with 1×10^6 $TCID_{50}$/cell MOI of JEECV. At 10 days p.i., DNA is extracted from gills. DNA is also extracted from gills of eel with natural VECNE and healthy eel. Conventional PCR is performed using three different primers (primer set A: JEECV-A1 and -A2, set B: JEECV-B1 and -B2, set C: JEECV-C1 and -C2). M, 100-bp DNA ladder marker; lane 1, eels with natural VECNE; lane 2, JEECV-infected eels; and lane 3, healthy eel.

reaction mixture contained 1× GoTaq Master Mix, 1 μl each of 50 μM forward and reverse primers, and template DNA. Primers are as follows:

004A-1 (5′-GGTCTCATGAAATGTAGATGTGCAGGTTAA-3′) and
004A-2 (5′-AATGCATATGAACGAGATATATACGAGC-3′) for 100-bp PCR products;
004C-1 (5′-CTCTCCGCCCTCCTGCTCATCCGGCTC-3′) and
004C-2 (5′-AATCAGACGCGCCTGAGCAGACCCAGCT-3′) for 110-bp PCR products;
024-1 (5′-TGTGATTTAGCGCAACGGCCGCAGCATA-3′) and
024-2 (5′-AGGCATCGCACATTAAACTGCACGCGCA-3′) for 240-bp PCR products; and
024-3 (5′-TACTGGTGTCTATTTGTTGCCGCACCTGC-3′) and
024-4 (5′-CAACGAACCCCGTAATTGGAATAAAGCGT-3′) for 121-bp PCR products. Usually, each PCR cycle involved denaturing at 94 °C for 2 min, annealing at 55 °C for 30 s, and primer extension at 72 °C for 30 s. This reaction was performed for 30–40 cycles. The nucleic acid sequences of PCR products were confirmed by direct sequencing.

For overlapping PCR, we used the iProof HF long PCR system (BioRad, USA). The reaction mixture contained 1× master mix, 0.2 μl each of 50-μM forward and reverse primers, and template DNA. Primers are as follows:

162F (5′-TCTGAATGCAATGTATGACTGAGATCC-3′) and
2821R (5′-ATCTGAGCTGCTGCGCCCAGGAAAGCTGG-3′) for 2659-bp PCR products;
2682F (5′-GACGCTTATGACGCTCCACTGGATGCGCAT-3′) and
6011R (5′-CTCTGCCATCTGAAGCCTCTTGCGCGTACC-3′) for 2940-bp PCR products;
5622F (5′-GGGACGTACCAGCGGAAGTACACACAATGA-3′) and
9011R (5′-TCACTCAAGCACAGGCTATGGACCAGCCCC-3′) for 3389-bp PCR products;
8382F (5′-TCAGTCATGCCGCCTGTAGAAAGCACCTG-3′) and
12011R (5′-ACGCCCCCCATGCCTGACCCTATGTTCGG-3′) for 3629-bp PCR products;
11142F (5′-GTCATACGTCCGTGCGCTGCCCTGAGGAAC-3′) and
15011R (5′-TTTATGAAGGAAGTAATATGTGTTTAATTC-3′) for 3869-bp PCR products;
371R (5′-CAAGTATGAGTCATTTCAATTGTATGAGCC-3′) and
14442F (5′-AGTTCTGTGACCACTGATCCCAGCTTAG-3′) for 1240-bp PCR products.

Each PCR cycle consisted of 98 °C for 30 s, followed by denaturing at 98 °C for 5 s, annealing at 55 °C for 15 s, and extension at 72 °C for 15 min. This reaction was performed for 35 cycles. The nucleic acid sequences were confirmed by direct sequencing.

For PCR with high sensitivity, we used AmpliTaq Gold Master (Applied Biosystems). The reaction mixture contained 1× master mix, 0.5 μl each of 50-μM forward and reverse primers, and template DNA. Primers are as follows (Fig. 3B):

JEECV-A1 (5′-GACGGTCCTAAACATGAACGGTGAAATGTC-3′) and
JEECV-A2 (5′-GGTATTTTGTACTCATTCATAGTGGCAATC-3′) for 270 bp as primer set A;
JEECV-B1 (5′-TGGGTGACCCCGAAGGGGCACTGTACG-3′) and
JEECV-B2 (5′-TATGTATAAACAGATTACGTGGCATACCTG-3′) for 240 bp as primer set B; and
JEECV-C1 (5′-TGCGCCCAGGCTTACCCTGTGCTCGATGTC-3′) and
JEECV-C2 (5′-CGGGCAGACGCAGACAACGCACTGCTGAAC-3′) for 330 bp as primer set C.

Each PCR cycle consisted of activation of Taq polymerase at 95 °C for 9 min, followed by denaturing at 95 °C for 30 s, annealing at 65 °C for 30s, and extension at 72 °C for 1 min. This reaction was performed for 70 cycles. The nucleic acid sequences were confirmed by direct sequencing.

RT-PCR

RNA was extracted from JEECV- and mock-infected cells at 3 days p.i. using an Isogen RNA extraction kit (Nippon Gene, Japan). To eliminate viral DNA from the RNA solution, RNA was repurified using a Total RNA Isolation Mini Kit (Agilent Technologies Inc., USA). Furthermore, Turbo DNA free was used to digest DNA completely. cDNA was synthesized using Superscript III (Invitrogen, USA) with random primers. As a control, the reaction was performed without Superscript III enzyme. PCR was performed using primers 024-2 and 024-5 (5′-TCAGGGTGGTCTGCTTCCGG-3′) using GoTaq (30 cycles). The size of PCR products was 503 bp.

Real-time PCR

The primers and probe were designed for a segment of the large T-antigen-like region. The primers are 025-1 (5′-TTGCCGCACC-TGCTTCAG-3′) and 025-2 (5′-CGAACACCGTAATTGGAATAAAGC-3′) for a 120-bp PCR product, and the probe is 025P (5′-FAM-ACACGC-TGCTCAAATTGCTGCTGCCT-TAMRA-3′). Serial dilution of known copies of JEECV DNA as a purified PCR product (primers 024F1 and 024R1) was used as standard DNA for real-time PCR. The TaqMan real-time PCR assay was performed in a 7500 Sequence Detection System using TaqMan Gene Expression Master Mix (Applied Biosystems) according to the instruction manual. For a time-course study of viral infection, DNA was extracted from the cells and supernatant using a QIAamp DNA mini kit. Three microliters of eluted DNA (total 50 μl) from supernatant and 10-ng eluted DNA from cells were used as templates. The thermal cycling profile of this assay comprised the following steps: 2 min at 50 °C, 10 min at 95 °C, followed by 45 cycles of PCR at 95 °C with denaturing for 15 s and at 60 °C for 1 min with annealing/extension for 1 min. The TaqMan assay was performed triplicate for each sample. DNA standards (copy number: 1 to 1×10^7) were used to construct a standard curve.

Southern blot analysis

Frozen cell pellets of virus-infected and uninfected cells were thawed and resuspended in 200-μl PBS (−). The samples were then frozen and thawed two more times followed by centrifugation with 13,000*g* at 4 °C for 10 min to produce pellets. The supernatant, approximately 200 μl, was extracted for DNA using the QIAamp MiniElute virus spin kit (Qiagen), and the extracted DNA was resuspended in 100 μl of buffer AVE. DNA (1.7 μg) was digested

using *BglII* for 4 h or not digested and run in 0.8% agarose gels. The probe used was the gel-purified PCR product using 2682F and 6011R primers, and the Megaprime DNA Labeling System (GE Healthcare) was used for ^{32}P-labeling. Hybridization was performed in ULTRAhyb (Ambion) with labeled probe at 42 °C for 15 h. Membrane washing was performed six times under the condition of 0.1× SSC and 0.1% SDS at 42 °C for 15 min. The signal was detected using X-ray film and Image analyzer (FLA2000, Fuji film, Japan).

Analysis using next generation sequencer

Viral DNA was extracted using a QIAamp DNA mini kit after precipitation using ultracentrifugation of 30-ml virus-infected supernatant (T-75 flask; Falcon) at 4 days p.i. The viral DNA was randomly amplified using Genomiphi V2 (GE Healthcare, USA) containing Phi29 enzyme, and single-stranded DNA was digested using S1 nuclease. The Genome Sequencer FLX System (Roche and 454 Life Sciences) was used in this study. DNA sequencing libraries were constructed and sequenced using Hokkaido System Science Ltd. The total number of reads was 17,000, and the total number of bases was 5,146,764. The read sequences were analyzed using GS *De novo* Assembler Version 2.3 (Roche) for *de novo* assembly.

Alignment of amino acid sequences

Nucleic acid sequences of JEECV were analyzed using BLASTx at NCBI. The polyomavirus large T-antigen-like region of JEECV was compared with that of polyomaviruses deposited in GenBank. Alignment was performed using MEGA4 software.

Acknowledgments

We thank Ms. Momoko Ogata of the National Institute of Infectious Diseases of Japan for her assistance. This study was supported in part by a grant from the Ministry of Education, Culture, Sports, Science, and Technology, Japan (#21580235 Scientific Research C:general). We are very grateful to the advice of Dr. Hiritaka Konuma, Tokai University, Drs. Hirokazu Kimura and Haruo Watanabe, National Institute of Infectious Diseases.

References

Bennett, M.D., Woolford, L., Stevens, H., Van Ranst, M., Oldfield, T., Slaven, M., O'Hara, A.J., Warren, K.S., Nicholls, P.K., 2008. Genomic characterization of a novel virus found in papillomatous lesions from a southern brown bandicoot (Isoodon obesulus) in Western Australia. Virology 376, 173–182.

Bennett, M.D., Reiss, A., Stevens, H., Heylen, E., Van Ranst, M., Wayne, A., Slaven, M., Mills, J.N., Warren, K.S., O'Hara, A.J., Nicholls, P.K., 2010. The first complete papillomavirus genome characterized from a marsupial host: a novel isolate from *Bettongia penicillata*. J. Virol. 84, 5448–5453.

Egusa, S., Tanaka, M., Ogami, H., Oka, H., 1989. Histopathological observations on an intense congestion of the gills in cultured Japanese eel, *Anguilla japonica*. Fish Pathol. 24, 51–56.

Inoue, K., Miwa, S., Aoshima, H., Oka, H., Sorimachi, M., 1994. A histopathological study on the etiology of intense congestion of the gills of Japanese eel, *Anguilla japonica*. Fish Pathol. 29, 35–41.

John, R., Muller, H., 2007. Polyomaviruses of birds: etiologic agents of inflammatory diseases in a tumor virus family. J. Virol. 81, 11554–11559.

Johne, R., Muller, H., Rector, A., van Ranst, M., Stevens, H., 2009. Rolling-circle amplification of viral DNA genomes using phi29 polymerase. Trends Microbiol. 17, 205–211.

Maeda, K., Hondo, E., Terakawa, J., Kiso, Y., Nakaichi, M., Endoh, D., Sakai, K., Morikawa, S., Mizutani, T., 2008. Isolation of a novel adenovirus from a fruit bat (*Pteropus dasymallus yayeyamae*). Emerg. Infec. Dis. 14, 347–349.

Mills, R., Rozanov, M., Lomsadze, A., Tatusova, T., Borodovsky, M., 2003. Improving gene annotation in complete viral genomes. Nucleic Acids Res. 31, 7041–7055.

Mizutani, T., Endoh, D., Okamoto, M., Shirato, K., Shimizu, H., Arita, M., Fukushi, S., Saijo, M., Sakai, K., Limn, C.K., Ito, M., Nerome, R., Takasaki, T., Ishii, K., Suzuki, T., Kurane, I., Morikawa, S., Nishimura, H., 2007. Rapid genome sequencing of RNA viruses. Emerg. Infec. Dis. 13, 322–324.

Ono, S., Nagai, A., 1997. Electronmicroscopic observation and experimental infection of congestion in gills of Japanese eel, *Anguilla japonica*. J. School Marine Sci. Technol. 43, 95–105.

Ono, S., Wakabayashi, K., Nagai, A., 2007. Isolation of the virus causing viral endothelial cell necrosis of eel from cultured Japanese eel, *Anguilla japonica*. Fish Pathol. 42, 191–200.

Pipas, J.M., 1992. Common and unique features of T antigens encoded by the polyomavirus group. J. Virol. 66, 3979–3985.

Sakai, K., Ueno, Y., Ueda, S., Yada, K., Fukushi, S., Saijo, M., Kurane, I., Mutoh, K., Yoshioka, K., Nakamura, M., Takehara, K., Morikawa, S., Mizutani, T., 2009. Novel reovirus isolation from an Ostrich (*Struthio camelus*) in Japan. Vet. Microbiol. 134, 227–232.

Tanaka, M., Satoh, T., Ma, W.J., Ono, S., 2008. Effectiveness of increasing temperature of rearing water and non-feeding against viral endothelial cell necrosis of eel. Fish Pathol. 43, 79–82.

Watanabe, S., Maeda, K., Suzuki, K., Ueda, N., Iha, K., Taniguchi, S., Shimoda, H., Kato, K., Yoshikawa, Y., Morikawa, S., Kurane, I., Akashi, H., (in press). Identification of a novel betaherpesvirus in bats using a rapid determination system for viral RNA sequences (RDV). Emerg. Infect. Dis.

Watanabe, S., Ueda, N., Iha, K., Masangkay, J.S., Fujii, H., Alviola, P., Mizutani, T., Maeda, K., Yamane, D., Walid, A., Kato, K., Kyuwa, S., Tohya, Y., Yoshikawa, Y., Akashi, H., 2009. Detection of a new bat gammaherpesvirus in the Philippines. Virus Genes 39, 90–93.

Woolford, L., Rector, A., Van Ranst, M., Ducki, A., Bennett, M.D., Nicholls, P.K., Warren, K. S., Swan, R.A., Wilcox, G.E., O'Hara, A.J., 2007. A novel virus detected in papillomas and carcinomas of the endangered western barred bandicoot (*Perameles bougainville*) exhibits genomic features of both the Papillomaviridae and Polyomaviridae. J. Virol. 81, 13280–13290.

Woolford, L., O'Hara, A.J., Bennett, M.D., Slaven, M., Swan, R., Friend, J.A., Ducki, A., Sims, C., Hill, S., Nicholls, P.K., Warren, K.S., 2008. Cutaneous papillomatosis and carcinomatosis in the Western barred bandicoot (*Perameles bougainville*). Vet. Pathol. 45, 95–103.

Woolford, L., Bennett, M.D., Sims, C., Thomas, N., Friend, J.A., Nicholls, P.K., Warren, K.S., O'Hara, A.J., 2009. Prevalence, emergence, and factors associated with a viral papillomatosis and carcinomatosis syndrome in wild, reintroduced, and captive western barred bandicoots (*Perameles bougainville*). EcoHealth 6, 414–425.

Yamao, T., Eshita, Y., Kihara, Y., Satho, T., Kuroda, M., Sekizuka, T., Nishimura, M., Sakai, K., Watanabe, S., Akashi, H., Rongsriyam, Y., Komalamisra, N., Srisawat, R., Miyata, T., Sakata, A., Hosokawa, M., Nakashima, M., Kashige, N., Miake, F., Fukushi, S., Nakauchi, M., Saijo, M., Kurane, I., Morikawa, S., Mizutani, T., 2009. Novel virus discovery from field-collected mosquito larvae using an improved system for rapid determination of viral RNA sequences (RDV ver4.0). Arch. Virol. 154, 153–158.

Chemistry & Biology
Article

Natural Product-Like Macrocyclic *N*-Methyl-Peptide Inhibitors against a Ubiquitin Ligase Uncovered from a Ribosome-Expressed De Novo Library

Yusuke Yamagishi,[1] Ikuo Shoji,[2] Shoji Miyagawa,[2] Takashi Kawakami,[1] Takayuki Katoh,[3] Yuki Goto,[3] and Hiroaki Suga[3,*]
[1]Department of Chemistry and Biotechnology, Graduate School of Engineering, The University of Tokyo, 7-3-1 Hongo, Bunkyo-ku, Tokyo 113-8656, Japan
[2]Division of Microbiology, Center for Infectious Diseases, Kobe University Graduate School of Medicine, 7-5-1 Kusunoki-cho, Chuo-ku, Kobe, Hyogo 650-0017, Japan
[3]Department of Chemistry, Graduate School of Science, The University of Tokyo, 7-3-1 Hongo, Bunkyo-ku, Tokyo 113-0033, Japan
*Correspondence: hsuga@chem.s.u-tokyo.ac.jp
DOI 10.1016/j.chembiol.2011.09.013

SUMMARY

Naturally occurring peptides often possess macrocyclic and *N*-methylated backbone. These features grant them structural rigidity, high affinity to targets, proteolytic resistance, and occasionally membrane permeability. Because such peptides are produced by either nonribosomal peptide synthetases or enzymatic posttranslational modifications, it is yet a formidable challenge in degenerating sequence or length and preparing libraries for screening bioactive molecules. Here, we report a new means of synthesizing a de novo library of "natural product-like" macrocyclic *N*-methyl-peptides using translation machinery under the reprogrammed genetic code, which is coupled with an in vitro display technique, referred to as RaPID (random nonstandard peptides integrated discovery) system. This system allows for rapid selection of strong binders against an arbitrarily chosen therapeutic target. Here, we have demonstrated the selection of anti-E6AP macrocyclic *N*-methyl-peptides, one of which strongly inhibits polyubiqutination of proteins such as p53.

INTRODUCTION

Peptides discovered as natural products share structural features that are not seen in ordinary polypeptides (proteins) expressed by the translation apparatus. Such "nonstandard" peptides are often macrocyclized and *N*-methylated in the backbone (Chatterjee et al., 2008); moreover, some of their side chains are modified to noncanonical functional groups or epimerized to *D*-configuration (Grünewald and Marahiel, 2006; Kohli et al., 2002; Li and Roller, 2002). These features concede critical biological and pharmacological properties, such as high affinity to binding partners, proteolytic resistance, and membrane permeability, and thus increase their specific potencies in vivo (Biron et al., 2008; Doedens et al., 2010; Driggers et al., 2008; Nestor, 2009; Sagan et al., 2004). Most of these peptides are produced by nonribosomal peptide synthetases (Grünewald and Marahiel, 2006; Kohli et al., 2002; Li and Roller, 2002) or are derived from ribosomally expressed peptides by enzymatic posttranslational modifications (Chatterjee et al., 2005; McIntosh et al., 2009; Oman and van der Donk, 2010). Despite the fact that libraries of "natural product-like" nonstandard peptides could be a very attractive source for drug discovery campaigns, the mechanistic and functional complexities of their production systems have been making it difficult for researchers to degenerate the sequences and lengths of nonstandard peptides and build their de novo library. Therefore, we have not yet witnessed a successful outcome of the generation of a highly complex "human-made" library and the discovery of novel peptide sequences against therapeutic targets.

Here, we report a unique means of synthesizing a "natural product-like" peptide library using a custom-made translation apparatus under the reprogrammed genetic code. The peptides in the library have the features of macrocyclic and *N*-methylated backbone along with a *D*-amino acid involvement in the sequences. Moreover, the library could be coupled with an in vitro display, and thus over a trillion members of nonstandard peptides can be rapidly screened against a chosen target. We referred to this platform system as RaPID (random nonstandard peptides integrated discovery) system. As a showcase of this system, we have performed selection of anti-E6AP macrocyclic *N*-methyl-peptides, and one of the abundant classes of selected peptides exhibited an inhibitory activity against E6AP-catalyzed polyubiquitination of target proteins, such as p53 and peroxiredoxin 1. Thus, the present work demonstrates a proof-of-technology and potentials of the RaPID system for the discovery of a novel class of nonstandard peptides against not only an E3 Ubquitin ligase but also previously nondruggable target families.

RESULTS AND DISCUSSION

Design of a Nonstandard Peptide Library Used in the RaPID System

The methodology of genetic code reprogramming, where arbitrary codons are reassigned from proteinogenic amino acids to nonproteinogenic amino acids, allows us to express "nonstandard" peptides using a translation apparatus (Forster et al., 2003; Josephson et al., 2005; Ohta et al., 2007; Ohta et al., 2008). To facilitate such a reprogramming, we have

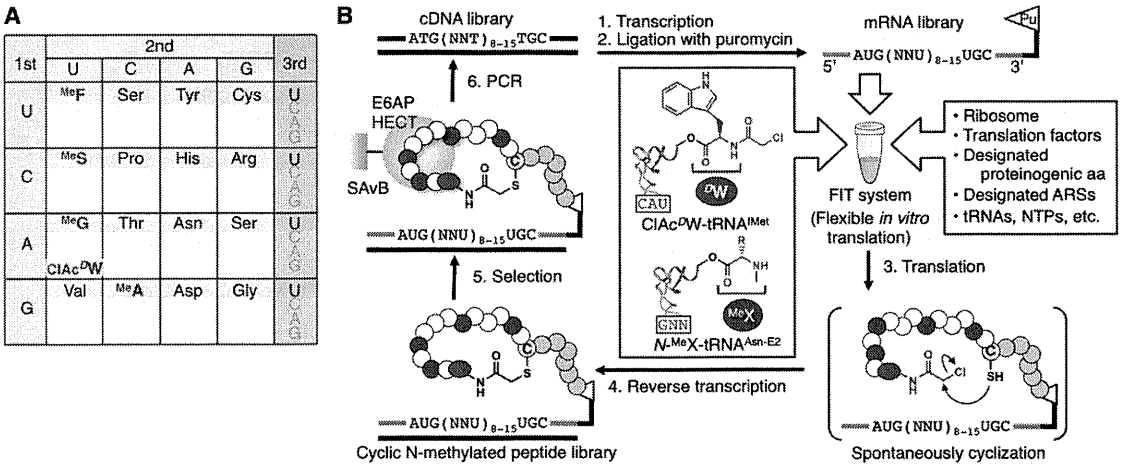

Figure 1. In Vitro Selection of Macrocyclic *N*-Methylated Peptides against E6AP HECT Domain by RaPID System

(A) The genetic code reprogrammed for this study. Four *N*-methyl-amino acids (^{Me}F, ^{Me}S, ^{Me}A, and ^{Me}G) and chloroacetyl-*D*-tryptophan (ClAc^{D}W) are shown in red and blue, respectively.

(B) Overview of the RaPID system for the selection of macrocyclic *N*-methyl-peptides. Messenger RNA libraries containing random sequence domain, $(NNU)_{8-15}$, were transcribed from the corresponding cDNA library and were conjugated with an oligonucleotide bearing a 3′-puromycin residue. The resulting mRNAs were translated by FIT system in the presence of the appropriate aminoacyl-tRNAs prepared by flexizymes. Linear peptides displayed on the individual mRNAs were spontaneously cyclized after translation, and the resulting macrocyclic peptides are displayed. The peptide libraries were then subjected to biotin-Avi-$(His)_6$-GB1-HECT immobilized on streptavidin magnetic beads (SAvB), and active species are isolated. Reverse transcription was performed after the selection in the first round and before the selection from the second round. The cDNAs on active mRNA-peptide fusion were recovered and amplified by PCR.

developed the FIT (flexible in-vitro translation) system (Goto et al., 2011). This system involves a custom-made *Escherichia coli* reconstituted cell-free translation system (Kung et al., 1977; Shimizu et al., 2001), where arbitrary amino acids and cognate aminoacyl-tRNA synthetases (ARSs) can be omitted to make the corresponding codons vacant, to which nonproteinogenic amino acids are assigned by supplementing the corresponding aminoacyl-tRNAs prepared by the flexizyme (flexible tRNA acylation ribozyme) technology (Murakami et al., 2006; Ohuchi et al., 2007). In fact, by using a customized FIT system, we were able to express macrocyclic *N*-methyl-peptides under the genetic code reprogrammed with more than four kinds of *N*-methyl-amino acids (Kawakami et al., 2008). To construct highly diverse libraries of nonstandard peptides and to effectively screen them for designated bioactivity, the FIT system was further integrated with an in vitro display method, so-called mRNA display (Nemoto et al., 1997; Roberts and Szostak, 1997). By this integration, nonstandard peptides expressed by the FIT system would be covalently ligated to the respective mRNAs via puromycin, displaying nonstandard peptides for the desired activity panning. We referred this mRNA display system integrated with FIT system to as RaPID (random nonstandard peptides integrated discovery) system.

In the present work, we assigned five nonproteinogenic amino acids, *N*-(2-chloroacetyl)-*D*-tryptophan (ClAc^{D}W), *N*-methylphenylalanine (^{Me}F), *N*-methylserine (^{Me}S), *N*-methylglycine (^{Me}G), and *N*-methylalanine (^{Me}A), to AUG, UUU, CUU, AUU, and GCU codons by the addition of ClAc^{D}W-tRNA$^{fMet}_{CAU}$, ^{Me}F-tRNA$^{Asn\text{-}E2}_{GAA}$, ^{Me}S-tRNA$^{Asn\text{-}E2}_{GAG}$, ^{Me}G-tRNA$^{Asn\text{-}E2}_{GAU}$, and ^{Me}A-tRNA$^{Asn\text{-}E2}_{GGC}$, respectively, prepared by the flexizyme technology (Figure 1A). A mRNA library was constructed to have NNU codon (N represents any of four bases, A, G, C, and U) with the mixture of repeats from eight to 15, $(NNU)_{8-15}$; thereby, *N*-methyl-amino acids would randomly appear in this region with the lengths of eight to 15 residues. In right downstream of the random region, UGC that assigns cysteine (Cys) was installed. Because all expressed peptides should have a ClAc^{D}W at the N terminus assigned by AUG start codon, the ClAc group would intramolecularly react with the sulfhydryl group of the Cys residue assigned by UGC or potentially UGU appeared in the random region, macrocyclizing their backbone via a nonreducible thioether bond (Goto et al., 2008; Kawakami et al., 2008). Following the UGC codon, three repeats of (GGC)(AGC) encoding $(Gly\text{-}Ser)_3$ followed by UAG stop codon are embedded. The 3′ common sequence would facilitate the display of macrocyclic *N*-methyl-peptides on the respective mRNA molecules via the $(Gly\text{-}Ser)_3$-puromycin linkage (Figure 1B).

Three critical notes should be given for securing a high quality of the macrocyclic *N*-methyl-peptide library: (1) In this FIT system, the amino acids and their cognate ARSs, whose codons were reprogrammed (F, L, I, and A), were omitted from the translation components, minimizing the unwanted incorporation of these proteinogenic amino acids competing with the *N*-methyl-amino acids. Similarly, those unassigned by NNU codons (Q, K, E, and W) were omitted. Moreover, release factor-1 (RF1) was withdrawn to aim at halting elongation at UAG codon and thus increasing the efficiency of puromycin-peptide fusion. (2) Because four of 16 codons assigned by the NNU mRNA library encode *N*-methyl-amino acids, one *N*-methyl-amino acid residue would appear in every four residues by chance. Our previous studies suggested the thioether macrocyclization takes place cleanly in nearly quantitative manner, regardless of the length and composition of peptide

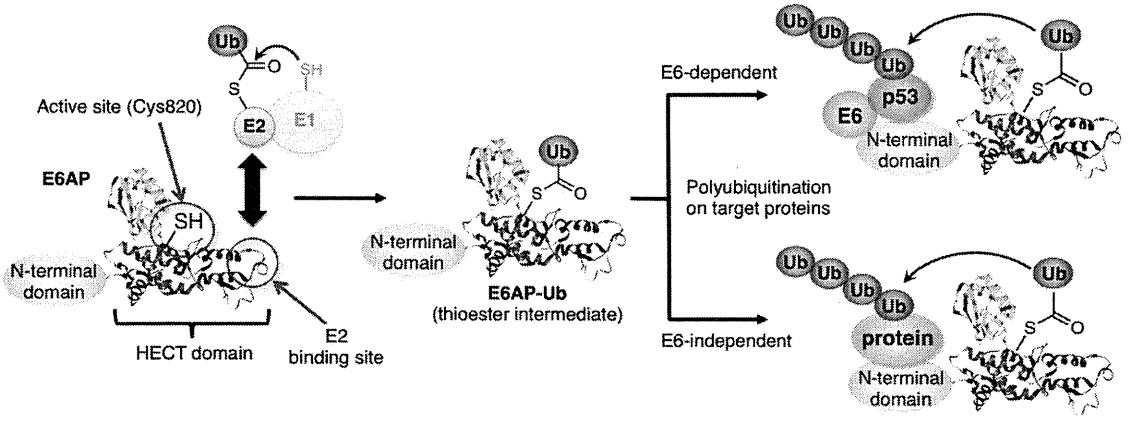

Figure 2. E6AP-Catalyzing Polyubiqutination of Target Proteins in E6-Independent and -Dependent Manners
In general, ubiquitin-activating enzyme E1 delivers an ubiquitin molecule (Ub) onto ubiquitin-conjugating enzyme E2 via a thioester linkage, and then Ub on E2 is transferred to ubiquitin ligase E3 forming a conjugate, E3-Ub. E6AP HECT (homologous to E6-associated protein [E6AP] C-terminus) domain (PDB 1C4Z), belonging to a member of E3 protein family, cooperatively catalyzes polyubiquitination on certain proteins, such as p53, with E6 (E6-dependent pathway) or directly polyubiquitinates various target proteins (E6-indendent pathway).

sequences (Goto et al., 2008; Kawakami et al., 2008). Moreover, because no stop codon was encoded in the $(NNU)_{8-15}$ random region, the highly reliable macrocyclic *N*-methyl-peptide library could be displayed by RaPID system. (3) The initial mRNA library consists of greater than 6×10^{12} unique members. It should be noted that the complexity of $(NNU)_{8-15}$ mRNA library should almost directly reflect to the peptide library complexity because only Ser is redundant in the genetic triplets used. Because the generally observed yield of mRNA-peptide fusion in the FIT system was 30% or more of the total input of mRNA, the diversity of the initial RaPID display library was estimated to be 10^{12} or more.

RaPID Selection against E6AP HECT Domain

The ubiquitin-proteasome system regulates the degradation of cellular proteins through enzyme cascade consisting of ubiquitin-activating enzyme E1, ubiquitin-conjugating enzyme E2, and ubiquitin (Ub) ligase E3 (Figure 2) (Hershko and Ciechanover, 1998; Pickart, 2001). Many families of E3 Ub ligases are known and are responsible for specific conjugation of polyubiquitins (polyUbs) to designated proteins, directing them to proteasome and thus triggering their proteolysis. Misregulation of the proteolysis of certain proteins caused by malfunction of E3 family ligases influences their downstream signal transduction processes, and therefore causes human disorders such as cancer (Hoeller et al., 2006) and neurodegeneration (Layfield et al., 2005; Rubinsztein, 2006). Thus, these E3 Ub ligases could be attractive targets for new therapeutic intervention (Eldridge and O'Brien, 2010; Hoeller and Dikic, 2009; Nalepa et al., 2006). Homologous to E6AP C-terminus (HECT) domain belongs to a family member of E3, and its N terminus domain cooperates with the human papillomavirus (HPV) E6 protein originating from the high-risk virus types 16 and 18 (Beaudenon and Huibregtse, 2008; Scheffner et al., 1993). The resulting E6AP and E6 complex provides the specific E3 ligase activity in the transfer of polyUbs onto p53 for the promotion of degradation, inhibiting p53-dependent apoptosis pathways (Figure 2). Moreover, it has been discovered that E6AP ubiquitinates some endogenous human proteins, such as HHR23A (a human homolog of the yeast DNA repair protein Rad23) (Kumar et al., 1999) and PML (promyelocytic leukemia) tumor suppressor (Louria-Hayon et al., 2009), in an E6-independent manner, suggesting that it also promotes the degradation of tumor-associated proteins. Despite advances in understanding of the molecular mechanism and structural study for HECT domains of E6AP (Huang et al., 1999) and other related enzymes (Eletr and Kuhlman, 2007; Ogunjimi et al., 2005), to the best of our knowledge, no selective inhibitor against E6AP has been yet reported by means of high-throughput screenings. Therefore, the development of inhibitors against HECT domain remains a formidable challenge. We here chose E6AP as a previously nondruggable target and performed selection of anti-E6AP peptides using RaPID system.

E6AP HECT domain was expressed as a fusion protein with an Avi-$(His)_6$-tag followed by a solubility-enhancement tag GB1 (streptococcal B1 immunoglobulin-binding domain of protein G) (Liu et al., 2009; Zhou et al., 2001) at the N terminus. This protein construct, Avi-$(His)_6$-GB1-HECT, in which Avi domain was biotinylated during the expression, was immobilized on streptavidin magnetic beads (SAvB, Figure 1B). The library was applied to the protein beads, and the bound fractions were selected at 4°C in the first and second round (Figure 3A). From the third round, GB1-immobilized SAvB was used as the negative selection to remove GB1-binding peptides, and then the positive selection was performed at 37°C to enrich the population with specific binding activity against the HECT domain. In the sixth round, we observed a significant increase in recovery rate of active fractions (Figure 3A), and therefore the resulting cDNA sequences in the pool were analyzed.

The sequence alignment of 47 clones revealed eight independent sequence families found in the pool 6 (Figure 3B). Six families, CM_{11}-1–6, are originating from the $(NNU)_{11}$ pool, whereas the remaining two families, CM_{13}-7 and CM_{13}-8, are from the $(NNU)_{13}$ pool. The most abundant sequence, CM_{11}-1, bearing four *N*-methyl residues, shares several common signatures of

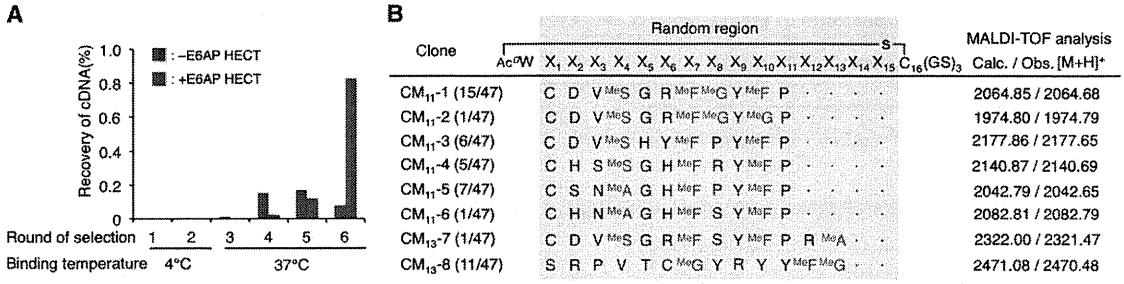

Figure 3. In Vitro Selection of Macrocyclic *N*-Methyl-Peptides against E6AP HECT Domain and Selected Active Species

(A) Progress of the selection. Recovery rates of cDNA from each round were estimated by recovered amounts over input amounts of cDNAs monitored by real-time PCR. The first and second rounds of selection were performed at 4°C, and the subsequent rounds were performed at 37°C. Those determined against SAvB•biotin-Avi-$(His)_6$-GB1-HECT as a positive selection are shown in blue, whereas those against SAvB•biotin-Avi-$(His)_6$-GB1 as a negative selection shown in red.

(B) Peptide sequences identified from the pool in round 6. The apparent frequency over a total number of clones and *N*-methyl amino acids of each sequence are shown in parentheses and red, respectively. The parental random region is highlighted in gray, in which a dot denotes a residue that did not appear in the random X_{12-15} region. Calculated (Calc.) and observed (Obs.) mass values ($[M+H]^+$) of each peptide expressed by FIT system are shown. See also Figure S1 and Table S1.

residues with other sequences. $^{Me}S_4$, G_5, $^{Me}F_7$, Y_9, $^{Me}F_{10}$, and P_{11} are highly conserved in CM_{11}-1–6 and CM_{13}-7, where four residues are notably the secondary amino acids. Among them, $^{Me}F_{10}\rightarrow$ $^{Me}G_{10}$ as well as $^{Me}S_4\rightarrow$ $^{Me}A_4$ substitutions were found in CM_{11}-2 and CM_{11}-5/CM_{11}-6, respectively, suggesting that the role of side chain group may be less important in activity but critical to be the *N*-methyl substituent. Moreover, $^{Me}G_8$ could be substituted with P_8 observed in abundant CM_{11}-3 and CM_{11}-5, whereas another abundant CM_{11}-4 and two other independent peptides CM_{11}-6–7 have R_8 and S_8, respectively. This may suggest that X_8 prefers to be the secondary amino acid but tolerates other amino acid substitutions. Mutations occurred during the course of selection is discussed more details in the Supplemental Information (see Figure S1 available online).

It is intriguing that the selection yielded only two lengths of *N*-methyl-peptides from the $(NNU)_{8-15}$ random region, given that other lengths of peptides should coexist in the initial pool, suggesting that the three-dimensional structure arisen from these two lengths might be critical to exhibit binding activity against E6AP HECT domain (Figure 3B). Importantly, the successful outcomes clearly demonstrated that the *N*-methyl-peptide library used in this study had a reliable quality and high complexity giving the *N*-methyl residues in the random region, and the RaPID system enabled us to select active species effectively and rapidly. The observed similarity in the composition of amino acid residues, particularly the positions as well as kinds of *N*-methyl residues appeared in the sequences, also suggests that specific interactions between the selected *N*-methyl-peptides and E6AP HECT domain are very likely occurring.

Characterization of Isolated Anti-E6AP Macrocyclic *N*-Methyl-Peptides

To confirm whether the identified mRNA sequences of CM_{11}-1–6 and CM_{13}-7–8 correctly produced the encoding macrocyclic *N*-methyl-peptides, we constructed the respective mRNA templates with a substitution of UAG with UAA that acts as a terminator of endogenous RF2 and performed in vitro expression using the same FIT system as the selection (Figure 3B, data in the column of MALDI-TOF analysis). MALDI-TOF analysis of the crude product expressed from the respective mRNA template showed a clean peak of which molecular mass is consistent with that calculated. This observation made us confident that the selected peptides had the *N*-methylated backbone as well as the composition of residues, as we expected from the cDNA sequences. For further characterization, we decided to focus on three abundant peptides, CM_{11}-1, CM_{11}-3, and CM_{11}-5, all of which consist of a total of 14 amino acid residues. The respective *N*-methyl-peptides were chemically synthesized by standard Fmoc solid-phase chemistry where the C terminus of G_{17} (corresponding to the 14th residue) was modified with carboxyamide (Table S1).

Because the above three peptides have a cysteine residue at position 1 (C_1) in the random region adjacent to $ClAc^DW$, cyclization between the ClAc group with C_1 side chain designated by UGU would potentially compete with that between the ClAc group with C_{16} side chain designated by UGC. To decipher which cyclization preferentially or selectively occurred, we synthesized three peptides based on CM_{11}-1 as a representative peptide; one is CM_{11}-1 itself, and the others are $C_1\rightarrow S_1$ mutant of CM_{11}-1 (CM_{11}-$1S_1$) and the corresponding to linear *N*-methyl-peptide by altering ClAc to acetyl (Ac) group, referred to as LM_{11}-1 (Table 1). Fragmentation of LM_{11}-1 by MALDI-TOF/TOF yielded peaks corresponding to linear fragments, as expected (Figure S2A). On the other hand, MALDI-TOF/TOF fragmentation of CM_{11}-1 and CM_{11}-$1S_1$ was much difficult than that for LM_{11}-1, and both gave similar fragmentation patterns (Figures S2B and S2C). Importantly, we were able to identify peaks corresponding to fragments containing the thioether linkage between the N-terminal acetyl group and the sulfhydryl group of C_{16} side chain in both CM_{11}-1 and CM_{11}-$1S_1$, but not between Ac and C_1 side chain in CM_{11}-1. These results well agree with the selective formation of the thioether linkage of Ac-S-C_{16}.

To evaluate the binding abilities of chosen peptides, CM_{11}-1, CM_{11}-3, and CM_{11}-5 (a series of these peptides are referred to as CM_{11}-peptides), we determined their kinetic and dissociation constants by means of surface plasmon resonance (SPR)

Table 1. Kinetic and Equilibrium Constants of Macrocyclic *N*-Methyl-Peptides against E6AP HECT Domain

Peptide	Sequence	k_{on} (x10^6) M^{-1}s^{-1}	k_{off} (x10^{-3}) s^{-1}	K_d nM
CM_{11}-1	$Ac^{D}WCDV^{Me}SGR^{Me}F^{Me}GY^{Me}FPCG$-$NH_2$ (S–C)	2.66	1.60	0.60
LM_{11}-1	$Ac^{D}WCDV^{Me}SGR^{Me}F^{Me}GY^{Me}FPCG$-$NH_2$	0.047	8.46	180
CM_{11}-1S_1	$Ac^{D}WSDV^{Me}SGR^{Me}F^{Me}GY^{Me}FPCG$-$NH_2$ (S–C)	1.33	15.5	11.7
CP_{11}-1	$Ac^{D}WCDV\ S\ GR\ F\ G\ Y\ F\ PCG$-$NH_2$ (S–C)	not detectable		>1000
LP_{11}-1	$Ac^{D}WCDV\ S\ GR\ F\ G\ Y\ F\ PCG$-$NH_2$	not detectable		>1000
CM_{11}-3	$Ac^{D}WCDV^{Me}SHY^{Me}F\ P\ Y\ ^{Me}FPCG$-$NH_2$ (S–C)	0.257	0.320	1.24
LM_{11}-3	$Ac^{D}WCDV^{Me}SHY^{Me}F\ P\ Y^{Me}FPCG$-$NH_2$	0.014	4.46	325
CM_{11}-5	$Ac^{D}WCSN^{Me}AGH^{Me}F\ P\ Y^{Me}FPCG$-$NH_2$ (S–C)	2.19	2.87	1.31
LM_{11}-5	$Ac^{D}WCSN^{Me}AGH^{Me}F\ P\ Y^{Me}FPCG$-$NH_2$	0.089	20.6	231

Data were collected by the standard SPR method using Biocore T100 and the constants were generated by the equipped data fitting program. See also Figures S2 and S3.

analysis against the E6AP Avi-$(His)_6$-GB1-HECT domain immobilized on a SAv-sensor chip (Table 1). All macrocyclic CM_{11}-peptides have values of k_{on} with a range of 0.2–3 × 10^6 $M^{-1}s^{-1}$, k_{off} with a range of 0.3–3 × 10^{-3} s^{-1}, resulting in the dissociation constants (K_d) with subnanomolar to 1 nM range. Thus, the representative CM_{11}-peptides studied here have remarkably strong affinity to E6AP HECT domain, and particularly CM_{11}-1 has the lowest K_d values among the CM_{11}-peptides. In addition to the CM_{11}-peptides, we synthesized the respective linear peptides bearing N-terminal acetyl group, referred to as LM_{11}-peptides. All LM_{11}-peptides lost affinity over 170-fold. This suggests that the macrocyclic structure closed by the Ac-S-C_{16} thioether bond in CM_{11}-peptides is crucial to exhibit high binding activity to the HECT domain.

In addition to the above peptides, we synthesized three more mutants of CM_{11}-1 to further validate the importance of the specific structure. One was the aforementioned $C_1 \rightarrow S_1$ mutant peptide, CM_{11}-1S_1, and the others are a macrocyclic peptide without N-methyl backbone but having the same side chains, CP_{11}-1, and its linear peptide, LP_{11}-1 (Table 1). CM_{11}-1S_1 had a 9-fold faster k_{off} rate than CM_{11}-1, implying that C_1 somehow contributes to slowing the dissociation from the target site but is not absolutely essential for binding activity. On the other hand, the other two mutants completely lost binding ability, indicating that *N*-methylated backbone with the N-terminal Ac-C_{16} thioether macrocycle is crucial to maintain the full binding capability of CM_{11}-1 against E6AP HECT domain.

Furthermore, we verified the binding specificity of CM_{11}-peptides against E6AP HECT domain using a different HECT-type E3 Ub ligase, Smurf2 (Ogunjimi et al., 2005). None of CM_{11}-peptides had any SPR signature of binding against Smurf2 Avi-$(His)_6$-GB1-HECT domain immobilized on a SAv-sensor chip, indicating that CM_{11}-peptides have high selectivity toward the E6AP HECT domain over Smurf2 HECT domain nor Avi-$(His)_6$-GB1-tag region (data not shown). Moreover, we investigated human plasma stability of CM_{11}-peptides compared with other control peptides (see more details in Supplemental Information and Figure S3), indicating that a CM_{11}-peptide (CM_{11}-1S_1) is very stable in plasma. Taken together, CM_{11}-peptides have remarkable binding activity and specificity to E6AP HECT domain and plasma stability.

CM_{11}-1 Inhibits Ubiquitination of Target Proteins Catalyzed by E6AP

Despite the observation of strong binding activity of CM_{11}-peptides to E6AP HECT domain, it does not necessarily mean that they are able to inhibit the E6AP ubiquitination activity. To assess whether CM_{11}-peptides have an ability to inhibit the ubiquitination activity, we chose the most active CM_{11}-1 and performed an in vitro assay to monitor ubiquitin thioester formation. It is known that E6AP or even its HECT domain alone forms the ubiquitin thioester intermediate (Beaudenon et al., 2005; Scheffner et al., 1990; Scheffner et al., 1995) in the presence of Ub, E1, and E2 in vitro (Figure 2). When an in vitro translation system from rabbit reticulocyte lysate (RRL), which contains these essential Ub-related components, was used for translating the E6AP HECT domain from the appropriate mRNA template in the presence of [^{35}S]-Met (Huibregtse et al., 1995),